Clouds, Aerosol, and Precipitation in the Marine Boundary Layer: An ARM Mobile Facility Deployment

Capsule: A 21-month deployment to Graciosa Island in the northeastern Atlantic Ocean is providing an unprecedented record of the clouds, aerosols and meteorology in a poorly-sampled remote marine environment

Robert Wood[1], Matthew Wyant[1], Christopher S. Bretherton[1], Jasmine Rémillard[6], Pavlos Kollias[2], Jennifer Fletcher[1], Jayson Stemmler[1], S. deSzoeke[3], Sandra Yuter[4], Matthew Miller[4], David Mechem[5], George Tselioudis[6], Christine Chiu[7], Julian Mann[7], Ewan O'Connor[7,18], Robin Hogan[7], Xiquan Dong[8], Mark Miller[9], Virendra Ghate[9], Anne Jefferson[10], Qilong Min[11], Patrick Minnis[12], Rabindra Palinkonda[13], Bruce Albrecht[14], Ed Luke[15], Cecile Hannay[16], Yanluan Lin[17]

[1]*Department of Atmospheric Science, University of Washington, Seattle WA*
[2]*McGill University*
[3]*Oregon State University*
[4]*North Carolina State University*
[5]*University of Kansas*
[6]*Columbia University*
[7]*University of Reading*
[8]*University of North Dakota*
[9]*Rutgers University*
[10]*NOAA CIRES*
[11]*SUNY Albany*
[12]*NASA Langley Research Center*
[13]*Science Systems and Applications, Inc., Hampton, Virginia.*
[14]*University of Miami*
[15]*Brookhaven National Laboratory*
[16]*National Center for Atmospheric Research*
[17]*Ministry of Education Key Laboratory for Earth System Modeling, Center for Earth System Science, Tsinghua University, Beijing, China*
[18]*Finnish Meteorological Institute, Finland*

ABSTRACT

The Clouds, Aerosol, and Precipitation in the Marine Boundary Layer (CAP-MBL) deployment at Graciosa Island in the Azores generated a 21 month (April 2009-December 2010) comprehensive dataset documenting clouds, aerosols and precipitation using the Atmospheric Radiation Measurement (ARM) Mobile Facility (AMF). The scientific aim of the deployment is to gain improved understanding of the interactions of clouds, aerosols and precipitation in the marine boundary layer.

Graciosa Island straddles the boundary between the subtropics and midlatitudes in the Northeast Atlantic Ocean, and consequently experiences a great diversity of meteorological and cloudiness conditions. Low clouds are the dominant cloud type, with stratocumulus and cumulus occurring regularly. Approximately half of all clouds contained precipitation detectable as radar echoes below the cloud base. Radar and satellite observations show that clouds with tops from 1-11 km contribute more or less equally to surface-measured precipitation at Graciosa. A wide range of aerosol conditions was sampled during the deployment consistent with the diversity of sources as indicated by back trajectory analysis. Preliminary findings suggest important two-way interactions between aerosols and clouds at Graciosa, with aerosols affecting light precipitation and cloud radiative properties while being controlled in part by precipitation scavenging.

The data from at Graciosa are being compared with short-range forecasts made a variety of models. A pilot analysis with two climate and two weather forecast models shows that they reproduce the observed time-varying vertical structure of lower-tropospheric cloud fairly well, but the cloud-nucleating aerosol concentrations less well. The Graciosa site has been chosen to be a permanent fixed ARM site that became operational in October 2013.

INTRODUCTION

The complex interactions among clouds, aerosols and precipitation are major sources of uncertainty in our ability to predict past and future climate change (Lohmann and Feichter 2005, Stevens and Feingold 2009, Quaas et al. 2009, Isaksen et al. 2009). Marine low clouds are particularly susceptible to perturbations in aerosols because they are spatially extensive (Warren et al. 1988), relatively optically thin (e.g. Turner et al. 2007, Leahy et al. 2012) and often form in pristine air masses (Platnick and Twomey 1994). Increases in aerosol concentrations due to anthropogenic emissions lead to increases in cloud droplet concentration that increase cloud brightness by increasing the overall surface area of droplets. These *aerosol indirect effects* (AIEs) are the dominant contributor to the overall aerosol radiative forcing in most climate models, yet are extremely poorly constrained and can vary by a factor of five across models (Quaas et al. 2009).

Climate models indicate that a major fraction of the global aerosol indirect radiative forcing signal is associated with marine low clouds (Quaas et al. 2009, and see Fig. 3 in Kooperman et al. 2012), which are poorly simulated in climate models (Zhang et al. 2005, Wyant et al. 2010). A range of models from simple theoretical models to sophisticated cloud resolving simulations all indicate that the Twomey effect (increased cloud reflectance stemming from the reduction of drop size by condensation on a larger number of nuclei) is by itself insufficient to explain how low clouds respond to changes in aerosols. They show that a significant fraction of the overall aerosol indirect effect may be related to precipitation suppression by aerosols and its impact upon the turbulent kinetic energy and moisture budget of the boundary layer (Albrecht 1989, Ackerman et al. 2004, Lohmann and Feichter 2005, Penner et al. 2006, Wood 2007). Because a significant fraction of the precipitation falling from low clouds

82 evaporates before reaching the surface (Comstock et al. 2004), this adds additional complexity to
83 the ways in which precipitation can impact cloud dynamical responses to aerosols.

84 Recent field measurements are shedding important new light on the factors controlling
85 precipitation rates in marine low clouds and particularly the role that aerosols may play in
86 suppressing it (Wood 2005, Geoffroy et al. 2008, Wood 2012, Terai et al. 2012). These studies
87 all show that, for a given amount of condensate or cloud thickness, precipitation from low clouds
88 decreases with increasing cloud droplet concentration. However, existing field datasets are
89 statistically limited by a relatively low number of cases. As such, it has proven challenging to
90 fully understand the role of precipitation suppression by aerosols. Spaceborne cloud radar
91 overcomes some of these sampling limitations and provides evidence that light precipitation is
92 susceptible to increased concentrations of droplets (e.g. Kubar et al. 2009, Wood et al. 2009) and
93 aerosols (L'Ecuyer et al. 2009). However, current spaceborne radar data suffer some limitations
94 such as low sensitivity, low vertical resolution and near-surface ground clutter contamination. In
95 addition, spaceborne aerosol column-integrated aerosol optical property retrievals do not
96 necessarily provide good constraints on cloud condensation nuclei concentrations (Liu and Li
97 2014). There is, therefore, a need to increase our surface sampling of aerosol-cloud-precipitation
98 processes using state-of-the-art remote sensing in conjunction with ground-based in situ
99 measurements of aerosol optical and cloud-forming properties.

100 The need for improved long-term but comprehensive measurements at a marine low
101 cloud site motivated the Clouds, Aerosol, and Precipitation in the Marine Boundary Layer (CAP-
102 MBL, *www.arm.gov/sites/amf/grw*) deployment of the Department of Energy Atmospheric
103 Radiation Measurement Mobile Facility (AMF) to the island of Graciosa in the eastern Atlantic
104 Ocean. Graciosa is a small island (~60 km^2 area) situated at 39.1°N, 28.0°W in the Azores

105 archipelago (Fig. 1), at a latitude that straddles the boundary between the subtropics and the
106 midlatitudes. As such, Graciosa is subject to a wide range of different meteorological conditions,
107 including periods of relatively undisturbed trade-wind flow, midlatitude cyclonic systems and
108 associated fronts, and periods of extensive low level cloudiness. Measurements were made from
109 April 2009 to December 2010.

110 CAP-MBL was designed to gather an extended record of high-quality data on clouds and
111 aerosol properties in a remote marine environment needed to improve the treatment of clouds
112 and aerosols in climate models. An important additional consideration for the deployment is the
113 ability to provide high-quality ground-based remote sensing and *in situ* data that can be used in
114 conjunction with spaceborne remote sensing to provide improved mapping and understanding of
115 the properties of marine low clouds over the remote oceans. The CAP-MBL deployment's
116 continuous record also allows for greater statistical reliability in the observed relationships
117 between aerosols, clouds and precipitation than is possible with aircraft, yet retains the
118 advantages of in-situ sampling of aerosol properties that are difficult to constrain with satellite
119 data. Table 1 lists the key science questions that the CAP-MBL deployment is designed to
120 address.

121 ## OBSERVATIONS

122 Table 2 details the suite of remote sensing instrumentation deployed as part of the campaign, and
123 Table 3 describes the *in situ* measurements. These tables also provide information describing the
124 physical variables derived from the instrumentation. The AMF measurements were all situated at
125 the airport on the northern, low-lying side of the island. Of all the instruments, perhaps most
126 important for CAP-MBL are the 95 GHz radar together with the ceilometer and the microwave
127 radiometer that together provide critical information on cloud boundaries, light precipitation, and

condensate amounts. The frequent soundings provide important information about MBL structure needed for model evaluation and to initialize process models. The cloud condensation nucleus counter, which is part of the ARM Aerosol Observing System is a critical measurement to provide constraints on the different aerosol influences on clouds. Figure 1 shows the location of the measurements on Graciosa and the broader Azores archipelago. In addition, during summer 2010, a small radiation platform was deployed at a trace-gas site established by NOAA close to the summit of the volcanic island of Pico (elevation 2350 m) some 60 km south of Graciosa (see e.g. Honrath et al. 2004). This suite included a Multi-filter Rotating Shadow-band Radiometer (MFRSR) and broadband shortwave and longwave radiometers. The scientific objective of this deployment was to measure the radiative fluxes and aerosol optical thickness above the marine boundary layer clouds and thereby provide a constraint that could be used in conjunction with surface radiation measurements at Graciosa to directly measure the cloud optical thickness in broken cloud fields.

The surface and in situ measurements are complemented by analyses of 3-km Meteosat-9 hourly images from the SEVIRI instrument using the visible-infrared-shortwave-infrared split window technique (see Minnis et al. 2011) over a domain bounded by 33°N, 43°N, 23°W, and 33°W. The SEVIRI analyses yield a variety of cloud and radiative properties including cloud cover, liquid water path, optical thickness, effective radius, cloud top temperature and height (Minnis et al. 2008).

CLOUD AND METEOROLOGICAL VARIABILITY

The specific CAP-MBL science questions (Table 1) include two focused on the impact of synoptic and seasonal variability on clouds and aerosols. To begin to address these, we note a marked seasonality in the surface pressure patterns near Graciosa (Fig. 2a,b). The winter season

151 exhibits a strong meridional gradient of surface pressure between the semi-permanent Icelandic
152 low and the Azores high (Fig. 2a). Surface winds are predominantly from the southwest in
153 January (Fig. 2c). The large values of the standard deviation of the 500 hPa geopotential height
154 over this region indicate a substantial amount of variability in the winter-season storm track
155 (Fig. 2a). Graciosa is usually either in the southern portion or to the south of individual winter-
156 season midlatitude cyclone tracks. This is reflected in the satellite cloud fraction data which
157 show a seasonal peak in total cloud fraction in the winter (Fig. 2e).

158 During summer, the Icelandic low disappears and the Azores high pressure system
159 strengthens (Fig. 2b), leading to reduced high and overall cloud cover (compare Figs. 2e and 2f,
160 also Fig. 3) and an increased prevalence of fair weather conditions. Surface wind speeds in July
161 are weaker than in winter and the wind direction ranges from southwesterly to northeasterly (Fig.
162 2d), depending upon the exact position of the Azores High. The prevalent surface high-pressure
163 conditions are associated with substantially reduced variability in the 500 hPa geopotential
164 height, implying that synoptic intrusions from high latitudes are far less frequent (Fig. 2b).

165 Figure 3a shows a time-height cross section of reflectivity from the vertically-pointing
166 W-band radar for the entire campaign, showing the range of conditions as a result of synoptic
167 and seasonal variability. Strong reflectivity at low levels, indicative of significant precipitation,
168 tends to occur during October to May and is often associated with relatively deep systems, in
169 some cases extending all the way to the tropopause. Interestingly, the seasonal cycle in the height
170 of the tropopause is strikingly evident. Low clouds are common through the entire year with an
171 annual average coverage of approximately 50% (Rémillard et al. 2012, Dong et al. 2013). The
172 primary modulation of the seasonal cycle of overall cloudiness is driven by high clouds
173 (Rémillard et al. 2012, Dong et al. 2013). Despite slightly fewer low clouds during summer

(more low liquid clouds are observed from space during summer, Fig. 2g,h, because of the reduced masking by high clouds), wintertime low clouds are frequently associated with deeper synoptic systems, and so the incidence of fair weather low clouds (stratocumulus and cumulus with no clouds above) is greatest in summer when the static stability is greatest (Rémillard et al. 2012, Dong et al. 2013). This makes the less disturbed summertime environment a more useful time to focus on the key science goals of CAP-MBL (Table 1), which will be easier to address when low clouds are exclusively present.

An analysis of the frequency of occurrence of different weather states derived through a cluster analysis of cloud property distributions (Fig. 4, based on Tselioudis et al. 2013), indicates that the Azores experience the range of different weather states with a similar frequency to that experienced globally. The Azores experience the low cloud weather states somewhat more frequently than the planet as a whole with fewer instances of clear skies and fair weather conditions, and more frequent occurrences of trade cumulus and stratocumulus, and this probably reflects the marine environment. The Azores also experience a range of middle and high level clouds that do not occur frequently in other stratocumulus regions, highlighting the complexity of the meteorological influences on clouds in the region. This is a result of the location of the Azores in the transition between the subtropical and midlatitude dynamic regimes, which also makes the location a particularly useful one to both study cloud changes in such dynamical transitions and to test the ability of models ranging from cloud resolving to GCM to simulate those cloud changes.

Although an excellent site for studying low clouds, Graciosa experiences a much greater degree of meteorological variability than is found in the subtropical stratocumulus sheets and the tropical trades that have been the subject of much recent research (e.g. Rauber et al. 2007,

Mechoso et al. 2013). This is exemplified by a common meteorological metric called the Estimated Inversion Strength (EIS), which is a bulk measure of the strength of the boundary layer capping inversion based on the average static stability between the surface and 700 hPa (Wood and Bretherton 2006). Figure 5 compares histograms of EIS summer when low cloud amount peaks, derived from CAP-MBL soundings with those from soundings taken from ships over the southeastern Pacific subtropical stratocumulus region during the peak low cloud season (austral spring) during VOCALS (de Szoeke et al. 2012). One can immediately see that during summertime Graciosa experiences a wider distribution of EIS values and a lower mean EIS than does the southeastern Pacific. There is actually very little overlap of the EIS distributions. The weaker inversions over Graciosa help explain why the low cloud cover during summer (~50%, Rémillard et al. 2012, Dong et al. 2013) is significantly less than that over the southeastern Pacific. The weaker and more variable inversions are also manifested in a much greater spread in the heights of summertime boundary layer clouds during summer over Graciosa compared with the southeastern Pacific region during VOCALS (Fig. 6).

AEROSOL AND CLOUD MICROPHYSICAL VARIABILITY AND AIR MASS ORIGINS

The Azores are influenced by a wide variety of air masses. The subtropical lower troposphere largely experiences conditions of large scale subsidence in which the MBL is continually being diluted by free-tropospheric (FT) air with a supply timescale of several days. The surface air therefore typically includes particles that have been entrained into the MBL over several days. It is therefore challenging to attribute the aerosol concentration measured at a given time to a single source. That said, daily trajectories during summer 2009 (Fig. 7) are useful for revealing the diversity of air masses arriving at Graciosa, which predominantly have North American,

220 subtropical Atlantic and north Atlantic origins if traced back 10 days. This diversity yields
221 strong variability in the concentration of cloud condensation nuclei (CCN). Some high CCN
222 concentration events can be traced back to trajectories passing over industrialized regions of
223 North America at low levels (Fig. 8b). Relatively high CCN concentrations indicative of
224 pollution influence can even be found in air masses that, according to trajectory analysis, have
225 been confined to the marine subtropical environment for the previous 10 days (Fig. 8a). This
226 likely occurs because the MBL entrained significant layers of pollution from the FT during its
227 excursion around the meandering subtropical high. Initial attempts to construct composite
228 trajectories for different aerosol loadings have not been fruitful because such a diverse range of
229 trajectories are found for any given loading. This indicates just how challenging it is to determine
230 how the synoptic meteorological variability impacts aerosols (Table 1).

231 Besides synoptic scale variability in aerosols at Graciosa, there are also interesting
232 seasonal variations in cloud and aerosol microphysical properties that are observed with a
233 number of different sensors. The CAP-MBL deployment provided the first opportunity for
234 comprehensive characterization of the seasonal variability in aerosol and cloud microphysical
235 properties in the Azores. Prior to this, it was known from gas phase measurements taken in the
236 free troposphere (FT) on Pico (Fig. 1b) that pollution and biomass burning aerosols from North
237 America frequently reach the remote North Atlantic region (Honrath et al. 2004) with a distinct
238 springtime maximum in the key indicator of combustion, carbon monoxide (Val Martin et al.
239 2008).

240 The seasonal cycle of cloud droplet concentration (N_d) estimates (Fig. 9a) shows a
241 spring/summer maximum and a minimum during winter, although different estimates yield
242 somewhat different annual cycles, an issue that needs further assessment by direct comparison of

retrievals for individual cases and by comparison with in situ data from aircraft. It is encouraging that all three N_d estimates have similar annual mean values and that the N_d cycle agrees qualitatively with the annual cycle of CCN concentration, especially at low supersaturations (Fig. 9b). This provides some preliminary evidence that the key processes involved in the Twomey effect are in operation in these clouds, which is one of the key scientific questions of CAP-MBL (Table 1). Determining the exact annual cycle of N_d using surface and satellite remote sensing requires a longer data record than is available from CAP-MBL and a more systematic comparison between different retrieval approaches than has been attempted thus far.

There are well-defined springtime peaks in submicron aerosol scattering (Fig. 9c) and AOD at Graciosa during CAP-MBL (Fig 9d). Boreal spring favors transport from industrialized continental areas, due to strong zonal westerlies and increased lofting of pollutants by cold fronts extending southward from midlatitude cyclones (Liang et al. 2004, Zhao et al. 2012). Although transport from continents is expected to be favored during the spring months, a picture consistent with the spring maximum in CO (Fig. 9d), there is also the possibility that reduced precipitation sinks during summertime also help to control the seasonal variability. Springtime aerosol maxima have also been observed over the Pacific at Mauna Loa (Bodhaine 1996, Andrews et al. 2012) and modeling studies indicate peak zonal intercontinental aerosol transport during Boreal springtime at all longitudes (e.g., Zhao et al. 2012). Aerosol extinction profiles derived from micropulse lidar during CAP-MBL show that the excess aerosol scattering in spring at Graciosa is confined below approximately 1 km altitude (Kafle and Coulter 2013). Supermicron aerosol scattering (difference between total and submicron scattering) exceeds the submicron scattering by a factor of 2-5 (Fig. 9c), with the greatest scattering during winter and spring, broadly consistent with greater sea-salt aerosol flux as wind speed increases (Fig. 2c,d).

Although the lack of enhanced FT scattering during springtime could lead one to conclude that long range transport is *not* responsible for the springtime maxima in aerosol loading at Graciosa, it is important to point out that free-tropospheric aerosols are typically smaller than those in the PBL and so their scattering signature is relatively weak and falls below the detection limit for spaceborne and most surface lidars. Despite this, when these particles are entrained into the PBL they grow due to aqueous phase deposition of sulfur species, and hygroscopically due to the high relative humidity in the boundary layer compared with the FT (Clarke et al. 2013). Aerosol single scattering albedo measurements during CAP-MBL (not shown) indicate that aerosols are more absorbing during springtime, consistent with the idea that combustion aerosols from North America are potentially influential on the remote Atlantic during this season.

PRECIPITATION AT GRACIOSA

Understanding the factors controlling precipitation, especially that falling from clouds in the MBL, is one of the main scientific questions being addressed by CAP-MBL (Table 1). Remarkably, the W-band radar shows that detectable precipitation echoes are present below cloud base for approximately half of all clouds at Graciosa (Rémillard et al. 2012). The near ubiquity of precipitation at the site is surprising given that the clouds are typically thin and often contain quite low condensate amounts. Precipitation at Graciosa is associated with clouds of all altitudes (Fig. 10a,b) such that clouds with top heights between 1 and 11 km all contribute roughly equally to surface precipitation in the annual mean. Even though low clouds produce relatively weak surface precipitation they occur in sufficient quantity (Fig. 10c) that their precipitation is climatologically important. In summertime, most precipitating clouds have tops lower than 5 km (Fig. 10b,c). Approximately 20% of the surface precipitation (~1 mm d^{-1} out of

289 an annual mean of ~5 mm d^{-1}) originates from clouds with tops below 3 km (Fig. 10a). During
290 the months of June-August, clouds with tops below 4 km contribute more than half of all surface
291 precipitation (Fig. 10b), and, surprisingly, this is also the case in late winter. The cumulative
292 contribution to precipitation as a function of quasi-instantaneous (30 s) rain rate (Fig. 10d)
293 indicates that 20% of precipitation accumulation is associated with conditional precipitation rates
294 lower than ~3 mm hr^{-1}. An accurate accounting of the precipitation climatology at Graciosa
295 must therefore include light precipitation from relatively shallow cloud systems.

296 ## INTERACTIONS BETWEEN CLOUDS, AEROSOLS, AND PRECIPITATION

297 A feature of the CAP-MBL deployment is the ability to simultaneously observe clouds, aerosols
298 and precipitation and to understand how these variables interact with each other. Interactions are
299 two way, with aerosols potentially impacting precipitation most likely via the suppression of
300 warm rain (Albrecht et al. 1989) but in turn aerosols are strongly scavenged by precipitation,
301 even in the relatively weak drizzle from low clouds (Wood 2006, Duong et al. 2011). Indeed,
302 climatological aerosol concentrations over the remote oceans may be determined by warm rain
303 processes (Wood et al. 2012). The CAP-MBL deployment's continuous record allows for greater
304 statistical reliability in the observed relationships between aerosols, clouds and precipitation than
305 is possible with aircraft, but retains the advantages of in-situ sampling of aerosol properties that
306 are difficult to constrain with satellite data. That said, the Azores exhibits stronger synoptic
307 variability than is found in the subtropical/tropical marine low clouds regions, making the
308 separation of aerosol effects on clouds from those caused by meteorological forcing somewhat
309 more challenging than in other regions dominated by low clouds. Because the summertime is
310 less synoptically variable and contains more single layer low clouds than the winter (Dong et al.
311 2014), it makes the summer a more productive starting point for analyses.

We illustrate a variety of aerosol-cloud-precipitation interactions using two case studies. First, we highlight a case where very low observed aerosol concentrations coincide with shallow, precipitating MBL clouds. Very low aerosol concentration events are a regular occurrence over the southeastern Pacific (Terai et al. 2013), where they tend to be associated with changes in the large-scale cloud morphology, and particularly the occurrence of open mesoscale cellular convection, which frequently occurs in the form of pockets or rifts within otherwise overcast stratocumulus (Stevens et al. 2005, Wood et al. 2008). According to a satellite-derived climatology, open mesoscale cellular convection occurs approximately 15% of the time during periods free of high clouds at the Azores (Muhlbauer et al. 2014). Factors controlling the preferred mesoscale morphology and transitions between different types of morphology is one of the key CAP-MBL science questions (Table 1). Figure 11 shows a case where a rift of open cells advects over Graciosa on 8-9 August 2009. The passage is marked by reductions in CCN concentrations that are close to an order of magnitude (Fig. 11b). Ship tracks can be seen in the satellite image within the rift, a region where SEVIRI retrievals show cloud droplet effective radii exceeding 20 μm (Fig. 11a). The ship tracks are also evident as lines of relatively small effective radius values in the rift (Fig. 11a). Immediately prior to the passage, clouds in the boundary layer were drizzling (Fig. 11e) although it is not clear if this precipitation influences the CCN concentrations in the rift itself. Strong aerosol depletion events have been observed in the tropics and subtropics (Clarke et al. 1998, Wood et al. 2008, Sharon et al. 2006, Petters et al. 2006) and in the Arctic (Mauritsen et al. 2011), with the likely cause in each case being precipitation scavenging. Strong CCN depletion events occur quite frequently at the Azores, and typically occur under conditions of light southerly winds and weak warm advection. It is important that we better understand the factors controlling the clean marine background aerosol

and its variability because climate model experiments show that the strength of the global aerosol indirect effect is strongly sensitive to the preindustrial aerosol conditions (Hoose et al. 2009, Ghan et al. 2013).

Figure 12 shows a case of overcast marine stratocumulus with variable precipitation over the course of four hours on 7 November 2010. CCN concentrations are fairly steady between 1245 and 1600 UTC. The cloud liquid water path (LWP) varies considerably, and appears to be a primary modulator of the cloud base precipitation rate including periods of virga as well as precipitation of several mm day^{-1} at its heaviest between 13 and 14 UTC. Interestingly, in the early part of the record shown in Fig. 12, the cloud droplet concentration and CCN levels are higher, so despite LWP values of 100-200 g m^{-2} between 12 and 13 UTC (similar to those between 14 and 15 UTC), little precipitation is falling. This is suggestive of a potential suppression of precipitation by increased aerosols as has been observed in other stratocumulus cloud regimes (Geoffroy et al. 2008, Sorooshian et al. 2010, Terai et al. 2012). Indeed, the entire CAP-MBL data record has been used to quantify the extent of this suppression (Mann et al. 2014), demonstrating the utility of the long AMF dataset for studying the influence of aerosols on precipitation.

CONFRONTING MODELS

A primary motivation for the Graciosa measurements is to facilitate the improvement of climate and weather forecast models. (Table 1). Other modeling groups are also making various uses of CAP-MBL data as detailed in Table 4.

The current skill of a few climate and weather forecast models in hindcasting clouds and aerosols at Graciosa is briefly analyzed below to illustrate the value of this approach for

357 comparing with the current measurements and to frame the opportunities for future improvement
358 of these models using more detailed analyses. The variety of clouds at Graciosa is a good test of
359 the moist physical parameterizations in these models. In addition, precipitation and cloud
360 processing can have major impacts on boundary layer aerosol concentration and size distribution.
361 Hence, for models with prognostic aerosols, a meaningful comparison of the simulated aerosol
362 with Graciosa observations requires a good simulation of the precipitation and cloud in the
363 region.

364 Operational global weather forecasts using the European Centre for Medium-Range
365 Weather Forecasts (ECMWF) and National Centers for Environmental Prediction (NCEP)
366 Global Forecast System models were sampled at the nearest grid point to the Graciosa site at
367 their native vertical resolution. Two global climate models (GCMs), the Community
368 Atmosphere Model (CAM) Version 5 and the Geophysical Fluid Dynamics Laboratory (GFDL)
369 Atmospheric Model Version 3.9, were run in a hindcast mode (Phillips et al. 2004). Five-day
370 global forecasts were initialized from daily 00UTC ECMWF analyses for June 1-Nov. 30 2009
371 interpolated to the climate model grid. The ECMWF analyses were produced for the Year of
372 Tropical Convection project at a resolution of ~25 km. The initial prognostic aerosol fields and
373 land surface characteristics for each GCM forecast were carried over from the previous 24 hour
374 forecast. In order to spin up these fields, daily hindcasts were also performed for the entire year
375 prior to the forecasts. The results we present use 24-48 hour forecasts, to avoid the initial spin-
376 up impacts from the ECMWF analysis.

377 Both climate models have much coarser horizontal grids than the weather forecast
378 models. Only the ECMWF model has a grid fine enough to begin to resolve Graciosa Island

379 itself. Hence, model errors in clouds and aerosols may arise not just from the simulated cloud
380 and aerosol physics but also from errors in the small-scale circulations and island-scale flow.

381 The CAM5 and GFDL models both use prognostic aerosol schemes including
382 representations of the interactions of clouds and aerosols. The ECMWF model also includes an
383 aerosol transport scheme, but it is not allowed to affect the physical forecasts. The NCEP model
384 does not include an aerosol scheme. We also did not archive accumulated precipitation or
385 vertically-resolved cloud cover from this model, so it could not be included in the plots below.

386 We analyze the simulated clouds and aerosols during a rainy month (November 2009)
387 and a dry month (August 2009). Figure 13 compares the accumulated precipitation over the
388 course of each month observed by the AMF tipping-bucket rain gauge with that predicted by the
389 12-35 hour ECMWF forecasts and the 24-48 hour forecasts for the two GCMs. This is a
390 necessarily imperfect comparison of a point measurement, possibly affected by the island terrain,
391 with a grid-cell mean value. Nevertheless, all the models are able to predict which days will be
392 relatively rainy, and their monthly accumulations lie within a factor of two of the observations.
393 This suggests that they capture most of the synoptic-scale variability that might be expected to
394 drive the day-to-day variations of clouds and aerosols, and furthermore, that hindcasts using the
395 climate models with interactive aerosol have a chance of simulating the effects of precipitation
396 scavenging on the aerosol population observed at Graciosa.

397 Figure 14 compares time-height sections of lower-tropospheric cloud cover simulated by
398 the three models with the cloud boundary product derived from the AMF vertically-pointing
399 cloud radar and lidar. During both months, all three models skillfully distinguish shallow and
400 deeper cloud regimes, though the AM3 cloud height appears less variable than observed during

401 the dry month (August). The periods with cloud extending above 4 km usually correspond to
402 rain events. These plots reiterate the potential for using a more in-depth comparison of global
403 models with this data set to improve their performance across a range of cloud types that is
404 different than sampled at long-running mid-latitude supersites in the U. S. and Europe.

405 Figure 15 compares aerosol sampled at ground level at Graciosa with that simulated by
406 the two climate models. The daily mean cloud condensation nucleus (CCN) concentration at a
407 supersaturation of 0.1% is shown, which we showed earlier (Fig. 9a,b) is a reasonable proxy for
408 the boundary-layer cloud droplet concentration. The models, like the observations, show higher
409 mean CCN in August than December, though both models tend to overestimate CCN on average.
410 During each of the two months shown, the observed CCN concentration varies by an order of
411 magnitude, and the models show similar overall levels of variability. The temporal correlation
412 coefficients of daily-mean log(CCN) between the models and the observations are positive for
413 both models during both months. However, they are not very large. Given $N = 30$ daily values,
414 with estimated 1-day lagged autocorrelation of $r_1 = 0.65$ for the models and $r_1 = 0.4$ for the
415 observations, the effective number of independent samples per month is
416 $N_* = N(1 - r_1 r_2)/(1 + r_1 r_2) = 18$ (Bretherton et al. 1999). With this sample size, the
417 correlation coefficient between a model and the observations must exceed 0.4 to be significant at
418 95% confidence using a one-sided test; each model exceeds this level in one of the two analyzed
419 months.

420 Overall, we conclude that the tested global models are simulating strong precipitation
421 events and the time-varying vertical cloud distribution at Graciosa fairly well, but aerosol
422 concentrations less skillfully. This suggests room for improvement in the parameterization of
423 aerosol processing by clouds, in marine aerosol sources, or errors in long-range aerosol transport.

By focusing on particular events, the Graciosa measurements should be useful for separating these sources of error to provide information specific enough to stimulate improvement of model simulations of aerosol, cloud and precipitation in remote marine regions.

SUMMARY AND FUTURE WORK

The observations collected during the 21- month CAP-MBL deployment of the AMF on Graciosa Island in the Azores comprise the longest dataset of its type collected to date in an extratropical marine environment. This paper described some of the key characteristics of the clouds, meteorology, aerosols and precipitation at the Azores, including the seasonal cycle, diverse range of air mass histories, strong synoptic meteorological variability compared with other low-cloud regimes, and important bidirectional interactions between aerosols, clouds and precipitation.

Although low clouds are the most frequently occurring cloud type, Graciosa is witness to a range of cloud types that are almost as diverse as those over the Earth as a whole, making the site an excellent choice for continued measurements by the ARM program. However, these ground-based measurements and retrievals must be validated by aircraft *in situ* measurements in order to provide a ground truth for validating the satellite observations and retrievals and to provide model evaluation data. In addition, the island site does not allow representative measurements of the surface heat and moisture fluxes over the ocean, but buoy measurements near Graciosa could potentially provide these. Given the great variety of aerosol, cloud and precipitation conditions, the data from CAP-MBL and from the permanent site (in operation late 2013) will continue to challenge understanding and provide an unprecedented dataset for the

446 evaluation and improvement of numerical models from cloud-resolving ones to global weather
447 and climate models.

448
449
450
451
452 **ACKNOWLEDGMENTS:**
453
454 The CAP-MBL deployment of the ARM Mobile Facility was supported by the U.S. Department
455 of Energy (DOE) Atmospheric Radiation Measurement (ARM) Program Climate Research
456 Facility and the DOE Atmospheric Sciences Program. We are indebted to the scientists and staff
457 who made this work possible by taking and quality-controlling the measurements. Data were
458 obtained from the ARM program archive, sponsored by DOE, Office of Science, Office of
459 Biological and Environmental Research Environmental Science Division. This work was
460 supported by DOE Grants DE-SC0006865MOD0002 [PI Robert Wood], DE-SC0008468 [PI
461 Xiquan Dong]; DE–SC0006736 [PI David Mechem], DE-SC0000991 [PI Patrick Minnis], DE-
462 SC0006712 [PI George Tselioudis], DE- SC0007233 [PI Christine Chiu], DE-SC0006701 [PI
463 Sandra Yuter]. The CloudSat data were distributed by the CloudSat Data Processing Center at
464 Colorado State University. MODIS data were obtained from the NASA Goddard Land Processes
465 data archive. VOCALS data were obtained from the Earth Observation Laboratory (EOL) at the
466 National Center for Atmospheric Research. The HYSPLIT IV model was obtained from the
467 NOAA Air Resources Laboratory. Data from the Aerosol Robotic Network (AERONET) were
468 obtained from the web download tool hosted by NASA Goddard Space Flight Center. The
469 National Center for Atmospheric Research is sponsored by the National Science Foundation.

REFERENCES

Ackerman A.S., Kirkpatrick, M.P., and Stevens D.E., Toon O. B., 2004: The impact of humidity above stratiform clouds on indirect aerosol climate forcing. *Nature*, **432**, 1014-1017.

Ahlgrimm, M., and R. Forbes, 2013: Improving the representation of low clouds and drizzle in the ECMWF model based on ARM observations from the Azores. Submitted to *Mon. Wea. Rev.*

Albrecht, B.A., 1989: Aerosols, Cloud Microphysics, and Fractional Cloudiness. *Science*, **245** (4923): 1227–30.

Andrews, E., J.A. Ogren, P. Bonasoni, A. Marinoni, E. Cuevas, S. Rodríguez, J.Y. Sun, D.A. Jaffe, E.V. Fischer, U. Baltensperger, E. Weingartner, M. Collaud Coen, S. Sharma, A.M. Macdonald, W.R. Leaitch, N.-H. Lin, P. Laj, T. Arsov, I. Kalapov, A. Jefferson, and P. Sheridan, 2011: Climatology of aerosol radiative properties in the free troposphere, *Atmos. Res*., **102**, 4, 365-393.

Bodhaine, B. A., 1996: Aerosol measurements during the Mauna Loa Photochemistry Experiment 2*, J. Geophys. Res.,* **101***,* 14757–14765*, doi:*10.1029/95JD02045.

Bretherton, C. S., M. Widmann, V. P. Dymnikov, J. M. Wallace, and I. Blade, 1999: Effective number of degrees of freedom of a spatial field. *J. Climate*, **12**, 1990-2009.

Burleyson, C. D., S. P. deSzoeke, S. E. Yuter, M. Wilbanks, and W. A. Brewer, 2013: Observations of the diurnal cycle of southeast Pacific marine stratocumulus clouds and precipitation. J. Atmos. Sci., 70, 3876-3894.

Chiu, J. C., A. Marshak, W. J. Wiscombe, S. C. Valencia, and E. J. Welton, 2007: Cloud optical depth retrievals from solar background "signal" of micropulse lidars. IEEE Geosci. Remote Sens. Lett, 4(3), 456–460, doi:10.1109/LGRS.2007.896722.

Clarke, A. D., et al., 1998: Particle nucleation in the tropical boundary layer and its coupling to marine sulfur sources. *Science*, **282**, 89– 92.

Clarke, A. D., S. Freitag, R. M. C. Simpson, J. G. Hudson, S. G. Howell, V. L. Brekhovskikh, T. Campos, V. N. Kapustin, and J. Zhou, 2013: Free Troposphere as the dominant Source of CCN in the Equatorial Pacific Boundary Layer: Long-Range Transport and Teleconnections. Submitted to *Atmos. Chem. Phys.*

499 Comstock, K. K., Wood, R., Yuter, S. E. and Bretherton, C. S.: Reflectivity and rain rate in and
500 below drizzling stratocumulus, Q. J. Roy. Meteor. Soc., 130(603), 2891–2918,
501 doi:10.1256/qj.03.187, 2004.
502 de Szoeke, S. P, S. Yuter, D. Mechem, C. Fairall, C. Burleyson, and P. Zuidema, 2012:
503 Observations of stratocumulus clouds and their effect on the eastern Pacific surface heat
504 budget along 20°S. *J. Climate*, 8542-8567.
505 Dong, X., T.P. Ackerman, and E.E. Clothiaux, 1998: Parameterizations of microphysical and
506 Shortwave radiative properties of boundary layer stratus from ground-based measurements. *J.*
507 *Geophys. Res*. 102, 31,681-31,393.
508 Dong, X., B. Xi, A. Kennedy, P. Minnis, and R. Wood, 2014: A climatology of marine aerosol-
509 cloud-radiation derived from the DOE ARM AMF deployment in the Azores: Part 1: Cloud
510 fraction and single-layered MBL cloud properties. *Journal of Climate*, in press.
511 Draxler, R. R., and G. D. Rolph, 2003: HYSPLIT (Hybrid Single-Particle Lagrangian Integrated
512 Trajectory) model, NOAA Air Resources Laboratory, Silver Spring, MD, USA,
513 http://www.arl.noaa.gov/ready/hysplit4.html.
514 Duong, H. T., Sorooshian, A., and Feingold, G., 2011: Investigating potential biases in observed
515 and modeled metrics of aerosol-cloud-precipitation interactions, *Atmos. Chem. Phys*., **11**,
516 4027-4037, doi:10.5194/acp-11-4027-2011, 2011.
517 Frisch, A. S., C. W. Fairall, and J. B. Snider, 1995: Measurement of stratus cloud and drizzle
518 parameters in ASTEX with a Ka-band doppler radar and a microwave radiometer. J. Atmos.
519 Sci., 52, 2788–2799.
520 Geoffroy, O., Brenguier, J.-L., and Sandu, I., 2008: Relationship between drizzle rate, liquid
521 water path and droplet concentration at the scale of a stratocumulus cloud system, *Atmos.*
522 *Chem. Phys*., **8**, 4641-4654, doi:10.5194/acp-8-4641-2008.
523 Ghan, S. J., S. J. Smith, M. Wang, K. Zhang, K. Pringle, K. Carslaw, J. Pierce, S. Bauer, and P.
524 Adams, 2013: A simple model of global aerosol indirect effects, *J. Geophys. Res. Atmos*.,
525 118, 6688–6707, doi:10.1002/jgrd.50567.
526 Honrath, R. E., R. C. Owen, M. Val Martı´n, J. S. Reid, K. Lapina, P. Fialho, M. P. Dziobak, J.
527 Kleissl, and D. L. Westphal, 2004: Regional and hemispheric impacts of anthropogenic and

biomass burning emissions on summertime CO and O3 in the North Atlantic lower free troposphere, *J. Geophys. Res*., **109**, D24310, doi:10.1029/2004JD005147.

Hoose, C., J. E. Kristjánsson, T. Iversen, A. Kirkevåg, Ø. Seland, and A. Gettelman (2009), Constraining cloud droplet number concentration in GCMs suppresses the aerosol indirect effect, *Geophys. Res. Lett.*, **36**, L12807, doi:10.1029/2009GL038568.

Illingworth, A. J., and Coauthors, 2007: Cloudnet. *Bull. Amer. Meteor. Soc.*, **88**, 883–898.

Isaksen, I. S. A., and coauthors, 2009: Atmospheric composition change: Chemistry-climate interactions. Atmos. Environ., 43, 5138-5192.

Jefferson, A., 2010: Empirical estimates of CCN from aerosol optical properties at four remote sites, *Atmos. Chem. Phys.*, **10**, 6855-6861, doi:10.5194/acp-10-6855-2010.

Kafle, D. N. and R. L. Coulter, 2013: Micropulse lidar-derived aerosol optical depth Climatology at ARM sites worldwide. *J. Geophys. Res*., **118**, 7293–7308, doi:10.1002/jgrd.50536.

Kooperman, G. J., M. S. Pritchard, S. J. Ghan, M. Wang, R. C. J. Somerville, and L. M. Russell, 2012: Constraining the influence of natural variability to improve estimates of global aerosol indirect effects in a nudged version of the Community Atmosphere Model 5, J. Geophys. Res., 117, D23204, doi:10.1029/2012JD018588.

Kubar, T., D. L. Hartmann, and R. Wood, 2009: Understanding the importance of microphysics and macrophysics for warm rain in marine low clouds: Part I. Satellite observations. *J. Atmos. Sci*., **66**, 2953-2972

Leahy, L. V., R. Wood, R. J. Charlson, C. A. Hostetler, R. R. Rogers, M. A. Vaughan, and D. M. Winker, 2012: On the nature and extent of optically thin marine low clouds, J. Geophys. Res., 117, D22201, doi:10.1029/2012JD017929.

L'Ecuyer, T. S., W. Berg, J. Haynes, M. Lebsock, and T. Takemura, 2009: Global observations of aerosol impacts on precipitation occurrence in warm maritime clouds, *J. Geophys. Res*., 114, D09211, doi:10.1029/2008JD011273.

Liang, Q., L. Jaegle´, D. A. Jaffe, P. Weiss-Penzias, A. Heckman, and J. A. Snow, 2004: Long-range transport of Asian pollution to the northeast Pacific: Seasonal variations and transport pathways of carbon monoxide, *J. Geophys. Res*., **109**, D23S07, doi:10.1029/2003JD004402.

Liu, J., and Z. Li, 2014: Estimation of cloud condensation nuclei concentration from aerosol optical quantities: influential factors and uncertainties, *Atmos. Chem. Phys*., **14**, 471-483, doi:10.5194/acp-14-471-2014.

Lohmann U., Feichter J., 2005: Global indirect aerosol effects: A review. *Atmos. Chem. Phys*, **5**, 715.

Luke, E. P. and P. Kollias, 2013: Separating cloud and drizzle radar moments during precipitation onset using Doppler spectra. *J. Atmos. Oceanic Technol.*, **30**, 1656–1671.

Mann, J. A. L., J. C. Chiu, R. J. Hogan, E. J. O'Connor, T. S. L'Ecuyer, T. H. M. Stein, and A. Jefferson, 2014: Aerosol impacts on drizzle properties in warm clouds from ARM Mobile Facility maritime and continental deployments, *J. Geophys. Res. Atmos*., **119**, doi:10.1002/2013JD021339.

Mauritsen, T., J. Sedlar, M. Tjernström, C. Leck, M. Shupe, M. Martin, B. Sierau, S. Sjögren, P.O.G. Persson, I. M. Brooks and E. Swietlicki, 2011: An Arctic CCN-limited cloud-aerosol regime. *Atmos. Chem. and Phys.*, **11**, 165-173.

Mechoso, C. R., R. Wood, R. Weller, C. S. Bretherton, A. D. Clarke, H. Coe, C. Fairall, J. T. Farrar, G. Feingold, R. Garreaud, C. Grados, J. McWilliams, S. P. de Szoeke, S. E. Yuter, P. Zuidema, 2013: Ocean-cloud-atmosphere-land interactions in the Southeastern Pacific. *Bull. Amer. Meteorol. Soc.*, in press.

Minnis, P., S. Sun-Mack, D. F. Young, P. W. Heck, D. P. Garber, Y. Chen, D. A. Spangenberg, R. F. Arduini, Q. Z. Trepte, W. L. Smith, Jr., J. K. Ayers, S. C. Gibson, W. F. Miller, V. Chakrapani, Y. Takano, K.-N. Liou, Y. Xie, and P. Yang, 2011: CERES Edition-2 cloud property retrievals using TRMM VIRS and Terra and Aqua MODIS data, Part I: Algorithms. *IEEE Trans. Geosci. Remote Sens.*, **49**, *11*, 4374-4400.

Muhlbauer, A., I. McCoy, and R. Wood, 2014: Climatology of stratocumulus cloud morphologies: microphysical and radiative properties. *Submitted to J. Geophys. Res.*

O'Connor, E. J., R. J. Hogan and A. J. Illingworth., 2005: Retrieving stratocumulus drizzle parameters using Doppler radar and lidar. *J. Appl. Meteorol*., **44**, 14-27.

Penner, J. E., Quaas, J., Storelvmo, T., Takemura, T., Boucher, O., Guo, H., Kirkevåg, A., Kristjánsson, J. E., and Ø. Seland, 2006: Model intercomparison of indirect aerosol effects, Atmos. Chem. Phys., 6, 3391-3405, doi:10.5194/acp-6-3391-2006.

586 Petters, M. D., Snider, J. R., Stevens, B., Vali, G., Faloona, I., and Russell, L., 2006:
587 Accumulation mode aerosol, pockets of open cells, and particle nucleation in the remote
588 subtropical Pacific marine boundary layer, *J. Geophys. Res*., 111, D02206,
589 doi:10.1029/2004JD005694.

590 Phillips, T. J., and coauthors, 2004: Evaluating parameterizations in general circulation models:
591 climate simulation meets weather prediction. *Bull. Amer. Meteor. Soc.*, **85**, 1903–1915.

592 Platnick, S., and S. Twomey, 1994: Determining the susceptibility of cloud albedo to changes in
593 droplet concentration with the Advanced Very High Resolution Radiometer. *J. Appl. Meteor.*,
594 **33**, 334–347.

595 Platnick, S., et al., 2003: The MODIS cloud products: Algorithms and examples from
596 Terra, *IEEE Trans. Geosci. Remote Sens*., **41**, 459-473, doi:10.1109/TGRS.2002.808301.

597 Quaas, J., Ming, Y., Menon, S., Takemura, T., Wang, M., Penner, J. E., Gettelman, A.,
598 Lohmann, U., Bellouin, N., Boucher, O., Sayer, A. M., Thomas, G. E., McComiskey, A.,
599 Feingold, G., Hoose, C., Kristjánsson, J. E., Liu, X., Balkanski, Y., Donner, L. J.,
600 Ginoux, P. A., Stier, P., Grandey, B., Feichter, J., Sednev, I., Bauer, S. E., Koch, D.,
601 Grainger, R. G., Kirkevåg, A., Iversen, T., Seland, Ø., Easter, R., Ghan, S. J., Rasch, P. J.,
602 Morrison, H., Lamarque, J.-F., Iacono, M. J., Kinne, S., and Schulz, M.: Aerosol indirect
603 effects – general circulation model intercomparison and evaluation with satellite data, Atmos.
604 Chem. Phys., 9, 8697-8717, doi:10.5194/acp-9-8697-2009, 2009.

605 Rauber, R.M., B. Stevens, H.T. Ochs, C. Knight, B.A. Albrecht, A.M. Blyth, C.W. Fairall, J.B.
606 Jensen, S.G. Lasher-Trapp, O.L. Mayol-Bracero, G. Vali, J.R. Anderson, B.A. Baker, A.R.
607 Bandy, E. Burnet, J.L. Brenguier, W.A. Brewer, P.R.A. Brown, P. Chuang, W.R. Cotton, L. Di
608 Girolamo, B. Geerts, H. Gerber, S. Göke, L. Gomes, B.G. Heikes, J.G. Hudson, P. Kollias, R.P.
609 Lawson, S.K. Krueger, D.H. Lenschow, L. Nuijens, D.W. O'Sullivan, R.A. Rilling, D.C. Rogers,
610 A.P. Siebesma, E. Snodgrass, J.L. Stith, D.C. Thornton, S. Tucker, C.H. Twohy, and P. Zuidema,
611 2007a: Rain in shallow cumulus over the ocean. *Bull. Amer. Meteor. Soc.*, **88**, 1912–1928.

612 Remer, L. A., and Coauthors, 2005: The MODIS Aerosol Algorithm, Products, and
613 Validation. *J. Atmos. Sci.*, **62**, 947–973.

614 Rémillard, J., P. Kollias, E. Luke, and R. Wood, 2012: Marine boundary layer cloud
615 observations at the Azores. *J. Climate,* 25, 7381-7398.

Sorooshian, A., G. Feingold, M. D. Lebsock, H. Jiang, and G. L. Stephens, 2010: Deconstructing the precipitation susceptibility construct: Improving methodology for aerosol-cloud precipitation studies, *J. Geophys. Res.*, **115**, D17201, doi:10.1029/2009JD013426.

Sharon, T. M., Albrecht, B. A., Jonsson, H., Minnis, P., Khaiyer, M. M., VanReken, T. M., Seinfeld, J., and Flagan, R., 2006: Aerosol and cloud microphysical characteristics of rifts and gradients in maritime stratocumulus clouds, *J. Atmos. Sci*., **63**, 983–997.

Stevens, B., G. Vali, K. Comstock, R. Wood, M. VanZanten, P.H. Austin, C.S. Bretherton, D.H. Lenschow, 2005: Pockets of Open Cells (POCs) and drizzle in marine stratocumulus, *Bull. Am. Meteorol. Soc.*, **86**, 51-57.

Stevens, B., and G. Feingold, 2009: Untangling aerosol effects on clouds and precipitation in a buffered system. *Nature.* **461**:7264, 607-613.

Terai, C. R., R. Wood, D. C. Leon, and P. Zuidema, 2012: Does precipitation susceptibility vary with increasing cloud thickness in marine stratocumulus? *Atmos. Chem. Phys.*, **12**, 4567-4583, doi:10.5194/acp-12-4567-2012, 2012.

Terai, C. R., C. S. Bretherton, R. Wood, and G. Painter, 2013: Aircraft observations of five pockets of open cells sampled during VOCALS-REx. Submitted to *Atmos. Chem. Phys.*

Toledano, C., V. E. Cachorro, A. M. de Frutos, B. Torres, A. Berjon, M. Sorribas, and R. S. Stone, 2009: Airmass classification and analysis of aerosol types at El Arenosillo (Spain), *J. Appl. Meteorol. Climat*., **48**, 962–981, 2009.

Tselioudis, G., W. Rossow, Y. Zhang and D. Konsta, 2013: Global weather states and their properties from passive and active satellite cloud retrievals. *J. Clim.* in press.

Turner, D. D., and Coauthors, 2007: Thin liquid water clouds: Their importance and our challenge. *Bull. Amer. Meteor. Soc.*, **88**, 177–190.

Turner, D. D., 2007: Improved ground-based liquid water path retrievals using a combined infrared and microwave approach, *J. Geophys. Res.*, **112**, D15204, doi:10.1029/2007JD008530.

Val Martin, M., R. E. Honrath, R. C. Owen, and Q. B. Li, 2008: Seasonal variation of nitrogen oxides in the central North Atlantic lower free troposphere, *J. Geophys. Res*., **113**, D17307, doi:10.1029/2007JD009688.

Warren, S. G., C. J. Hahn, J. London, R. M. Chervin, and R. L. Jenne, 1988: Global distribution of total cloud cover and cloud types over ocean. NCAR Tech. Note NCAR/TN-3171STR, National Center for Atmospheric Research, Boulder, CO, 42 pp. 1 170 maps.

Wood, R., 2005: Drizzle in stratocumulus. Part I: Horizontal and vertical structure. *J. Atmos Sci.,* **62***,* 3011-3034.

Wood, R, 2006: The rate of loss of cloud condensation nuclei by coalescence in warm clouds. *J.Geophys. Res.*, **111**, D21205, doi:10.1029/2006JD007553.

Wood, R., and C. S. Bretherton**,** 2006: On the relationship between stratiform low cloud cover and lower tropospheric stability., *J. Clim.,***19**, 6425-6432.

Wood, R., 2007: Cancellation of aerosol indirect effects in marine stratocumulus through cloud thinning. *J. Atmos. Sci*., **64**, 2657-2669.

Wood, R., K. K. Comstock, C. S. Bretherton, C. Cornish, J. Tomlinson, D. R. Collins, and C. Fairall, 2008: Open cellular structure in marine stratocumulus sheets. J. *Geophys. Res.*, **113**, D12207, doi:10.1029/2007JD009371.

Wood, R., T. Kubar, and D. L. Hartmann, 2009: Understanding the importance of microphysics and macrophysics for warm rain in marine low clouds: Part II. Heuristic models of rain formation. *J.Atmos. Sci*., 66, 2973-2990.

Wood, R., 2012: Stratocumulus Clouds. *Mon. Wea. Rev*., **140**, 2373–2423.

Wood, R., D. Leon, M. Lebsock, J. Snider, A. D. Clarke. Precipitation driving of droplet concentration variability in marine low clouds. *J. Geophys. Res.,* **117***,* D19210, doi:10.1029/2012JD018305.

Wyant, M. C., Wood, R., Bretherton, C. S., Mechoso, C. R., Bacmeister, J., Balmaseda, M. A., Barrett, B., Codron, F., Earnshaw, P., Fast, J., Hannay, C., Kaiser, J. W., Kitagawa, H., Klein, S. A., Köhler, M., Manganello, J., Pan, H.-L., Sun, F., Wang, S., and Wang, Y., 2010: The PreVOCA experiment: modeling the lower troposphere in the Southeast Pacific, *Atmos. Chem. Phys.*, **10**, 4757-4774, doi:10.5194/acp-10-4757-2010.

Zhang, M. H., et al., 2005: Comparing clouds and their seasonal variations in 10 atmospheric general circulation models with satellite measurements, *J. Geophys. Res*., **110**, D15S02, doi:10.1029/2004JD005021.

674 Zhao, T. L., Gong, S. L., Huang, P., and Lavoué, D., 2012: Hemispheric transport and influence
675 of meteorology on global aerosol climatology, *Atmos. Chem. Phys*., **12**, 7609-7624,
676 doi:10.5194/acp-12-7609-2012.
677

678 # TABLES AND FIGURES

679

Table 1: The primary science questions addressed during CAP-MBL
• Which synoptic-scale features dominate the variability in subtropical low clouds on diurnal to seasonal timescales over the North East Atlantic? • Do physical, optical, and cloud-forming properties of aerosols vary with the synoptic features? • What is the variability in precipitation frequency and strength in the subtropical cloud-topped MBL on diurnal to seasonal timescales, and is this variability correlated with variability in aerosol properties? • Can we find observational support for the Twomey effect in clouds in this region? • Are observed transitions in cloud mesoscale structure (e. g. from closed cellular to open cellular convection) influenced by the formation of precipitation? • How well can state-of-the-art weather forecast and climate models (run in forecast mode) predict the day-to-day variability of cloud cover and its radiative impacts?

680

681

682

683

684

685 *Table 2: Key AMF remote sensing instrumentation deployed during the CAP-MBL deployment of*
686 *the ARM Mobile Facility at Graciosa from April 2009-December 2010*

Instrument	Key derived parameters	Resolution/Range	Availability
95 GHz Profiling Radar (WACR)	(i) Cloud and precipitation vertical structure (ii) Cloud top height (iii) Drizzle drop size distribution using both Doppler spectral measurements (Frisch et al. 1995, Luke and Kollias 2013) and with MPL below cloud base (O'Connor et al. 2005)	Res.: 43 m Time: 2 s Max range: 15 km	Operational 5 June 2009 to end No data 1-25 Sept 2010 (see Rémillard et al. 2012 for sampling statistics)
Ceilometer (VCEIL) and Micropulse Lidar (MPL)	(i) Cloud base height (ii) Cloud cover (iii) Precipitation profiling below cloud base (with radar) (iv) cloud visible optical thickness in all-sky conditions	Res.: 15-30 m Time: 30-60 s Max range: ~5 km	VCEIL operational 13 April 2009-end MPL operational 11 April 2009-end (see Rémillard et al. 20 12 for sampling statistics)
Microwave Radiometer (MWR) – 23/31/90 GHz	(i) Cloud liquid water path (ii) Column water vapor path	Time: 20 s	Operational 27 April 2009-end (see Rémillard et al. 20 12 for sampling statistics)
Radar Wind Profiler (RWP)	(i) horizontal wind profiles (ii) virtual temperature profiles	Time: 6 min	Operational 1 May 2009-end
Visible Spectral Radiometers: MultiFilter Rotating Shadowband Radiometer (MFRSR); Narrow Field of View Radiometer (NFOV); Sunphotometer	(i) Cloud visible optical thickness. Used to infer cloud microphysical properties (droplet concentration, effective radius) in combination with MWR (ii) Aerosol optical properties in clear skies	Time: 20 s (MFRSR)	MFRSR operational 5 May 2009-end NFOV operational 20 Aug 2009-end Sunphotometer operational 1 May 2009-18 April 2011
Atmospheric Emitted Radiance Interferometer (AERI).	Cloud liquid water path (LWP) estimates for thin clouds (combined with MWR, following Turner 2007)	Spectral: 3-19.2 μm with 3.3-36 nm resolution Time: 6 min	Operational Apr-Jun 2009 and Dec 2009-Dec 2010
Broadband Radiometers	Downwelling shortwave and longwave radiative fluxes used to constrain the surface energy budget	Time: 1 min	Operational 15 April 2009-end
Total Sky Imager (TSI)	Cloud coverage and type	Time: 30 s	Operational 14 April 2009-end when solar elevation > 5-10°

687

688
689

690 *Table 3: Key AMF in situ measurements obtained during the CAP-MBL deployment of the ARM*
691 *Mobile Facility at Graciosa from April 2009-December 2010*

Instrument	Key derived parameters	Resolution	Comments
Balloon-borne Sounding System (BBSS)	(i) Atmospheric profile of temperature, humidity and winds (ii) MBL depth (iii) Inversion strength	4 soundings daily (00, 06, 12, 18 UTC)	Operational 16 April 2009-end
Eddy Correlation Systems (ECOR)	Surface turbulent fluxes of latent and sensible heat	Time: 30 mins	Operational 15 April 2009-11 Oct 2010
Surface Meteorological Instruments	Surface temperature, humidity, pressure, winds, precipitation rate (optical rain gauge)	Time: 30 sec	Operational 15 April 2009-end Mounted on 10 m tower
Surface aerosol observing system	Total aerosol concentration > 10 nm diameter (CN counter);	1 minute	Operational 14 Apr 2009-end
	CCN spectra at seven supersaturations (nominally 0.1, 0.2, 0.3,0.5, 0.8, 1, 1.1%)	Step through supersaturations, each sampled for 5 minutes	
	Dry (low RH) and wet (scanning RH from 40-90%) aerosol scattering (total and hemispheric backscattering) at three wavelengths (450, 550 and 700 nm) with 1 and 10 micron size cut-off;	1 minute resolution of 30 minute cycles between sub 1 um and sub 10 um aerosol	
	Aerosol absorption (PSAP) at three wavelengths (450, 550 and 700 nm) wavelength	1 minute resolution of 30 minute cycles between sub 1 um and sub 10 um aerosol	

692

693

694

695

696

697

698

699

700

701

Table 4: Modeling Projects using AMF Azores datasets	
Modeling project	**Model type and research group**
High resolution modeling with explicit aerosol representation to examine detailed microphysical processes observed with WACR. Evaluation of new parameterization of clouds in climate models.	• DHARMA LES and GISS GCM • Andrew Ackerman and George Tselioudis [NASA GISS]
Cloud resolving model simulations in 2D and 3D at relatively low resolution for entire deployment period.	• System for Atmospheric Modeling (SAM) • Steve Krueger [U. Utah]
Eddy resolving and regional models for particular cases during deployment to examine relative importance of meteorology and aerosols in driving cloud and precipitation.	• COAMPS and/or WRF • David Mechem [U. Kansas]
Compare cloud, aerosol and precipitation properties extracted from global GCMs with in-situ measurements	• CAM5 and GFDL AM3p9 • Cecile Hannay [NCAR]; Yanluan Lin [GFDL]
Use selected cases to compare single column version of a climate model with a cloud resolving model to examine sensitivity of clouds to aerosols.	• CAM5 and LES • Joyce Penner [U. Michigan]
Use selected cases to evaluate turbulent mixing, microphysical process rates, and precipitation susceptibility in single column versions of a climate model.	• CAM5 and CAM-CLUBB • Robert Wood [U. Washington]

702
703
704
705

FIGURE CAPTIONS

Figure 1: (a) Map of Graciosa Island showing terrain elevation, and the location of the AMF site at the airport approximately 2 km west of the main town Santa Cruz de Graciosa. (b) Map showing the location of the Azores in the North Atlantic. Colors show the annual mean cloud droplet concentration for warm, overcast clouds as observed by the Moderate Resolution Imaging Spectroradiometer (MODIS) on the NASA Terra satellite. The Azores receives a diverse range of airmasses from North America, from the Arctic and from Northern Europe. (c) Photograph of the AMF site looking to the SE; (d) Map of the location of Graciosa (and Pico) in the Azores archipelago.

Figure 2: Mean 1000 hPa geopotential heights (color-filled contours) for (a) Jan. and (b) Jul. generated from the 0000 UTC ERA–Interim reanalysis fields (Dee et al. 2011). Contours of the standard deviation of the 500 hPa geopotential heights [in meters] are overlaid to indicate variability in the storm track. (c) and (d) represent surface wind roses for Jan. and July, respectively. (e)–(h) show maps of MODIS mean total and liquid phase cloud fraction for Dec., Jan., and Feb. (DJF) and Jun., Jul., and Aug (JJA) seasons. Cloud fraction is derived on 1°×1° areas averaged over each 3 month season for the years 2002-2012 using the Collection 51 Aqua MODIS Cloud Phase Infrared Day Histogram Counts product. Day and night observations are combined. The star in the cloud fraction panels denotes the location of Graciosa Island. A 3×3 pixel median smoothing filter was applied to the data to remove orbit swath edge sampling artifacts.

Figure 3: (a) height-time series of vertically-pointing W-band radar reflectivity for the entire deployment. Radar data for much of September 2010 are missing; (b) monthly low and high cloud cover determined using the WACR and ceilometer dataset as described in Rémillard et al. (2012).

Figure 4: Frequency of occurrence of different weather states determined using passive and active cloud sensors at the Azores (solid) and for the globe as a whole (dotted). From Tselioudis et al. (2013).

Figure 5: Histogram counts of estimated inversion strength (EIS, Wood and Bretherton 2006) in 1 K bins from summertime (June-August) CAP-MBL 2009 and 2010 soundings (stacked blue and red bars, respectively) and VOCALS 2008 (October-November, gray bars). Right axis shows cumulative distributions of EIS for all of CAP-MBL (blue line) and VOCALS (gray line).

Figure 6: Cloud occurrence frequency as a function of height for Graciosa during JJA (solid) and from the southeastern Pacific during the VOCALS field campaign (Burleyson et al. 2013).

Figure 7: Clusters of trajectories arriving at Graciosa during the summer period (May-August 2009) showing the three primary clusters representing North American, Arctic/Northern European, and recirculating Azores high flow. The Hysplit IV model (Draxler and Rolph, 2003) was employed and 10 day back trajectories ending at Graciosa 500 m above sea level were run every day for April-September 2009. NCEP GDAS meteorological data including model vertical velocity is used to determine the trajectory motion. A cluster analysis was then performed on the resulting back trajectory set (e.g., Toledano et al., 2009) and a three cluster solution was found to capture most of the variance.

Figure 8: (a)-(d) Four examples of 10 day airmass back trajectories (see Fig. 7 caption for details) arriving at Graciosa during May 2009, reflecting characteristic airmasses. Each of the four panels show the trajectory map (top) and height (below) with ticks every 12 hours. Central panel shows CCN supersaturation spectra time series measured at Graciosa during the same month.

Figure 9: Composite seasonal cycles (using all available data) of (a) cloud droplet concentration retrieved using the transmitted solar irradiance and microwave radiometer (MWR) LWP (squares, Dong et al. 1998), from the MPL solar background light (Chiu et al. 2007) and MWR (black line), and from MODIS (red line, 1x1^{o} box encompassing Graciosa, all years 2001-2010, Platnick et al. 2003); (b) Surface CCN concentrations at four supersaturations; (c) Aerosol total and submicron dry extinction. Boxes span the 25th and 75th percentiles of the data with red bars indicating medians and the crosses indicating means; (d) Monthly mean aerosol optical depth and 25/50/75th percentile values from the sunphotometer (CIMEL, red) and mean values from MODIS (black). The composite seasonal cycle of carbon monoxide (CO) measured at the Pico mountain station from 2002 to 2005 is also shown (see Val Martin et al. 2008).

764
765 **Figure 10**: Characteristics of precipitation reaching the surface at Graciosa. (a) Cumulative
766 contribution to surface precipitation accumulation from clouds with tops exceeding the value
767 shown on the abscissa, using different approaches. The solid line shows precipitation determined
768 by the raingauge and cloud top height estimated with WACR for columns that are not completely
769 attenuated and satellite-determined IR cloud top height from SEVIRI for attenuated columns.
770 Filled circles are from CloudSat; (b) composite seasonal cycle of precipitation from 21 months of
771 the deployment (blue bars), and the cloud top height corresponding to percentiles of total
772 precipitation accumulation. For example, the filled circles indicate the cloud top height for which
773 50% of the total precipitation is associated with shallower clouds; (c) cloud top height
774 distributions corresponding to 30 s periods where the surface precipitation exceeds 10 mm d^{-1}.
775 Black solid line shows cloud tops from the WACR only and the dotted line shows those from
776 WACR/SEVIRI merge, both for annual data. The red curve shows corresponding plot for JJA;
777 (d) contribution to surface accumulation from precipitation rates exceeding the abscissal value.

778 **Figure 11**: (a) MODIS visible image on 8 August 2009 (12:40 UTC) showing rift feature
779 containing small open cells and shiptracks in a shallow boundary layer about to cross Graciosa.
780 Overlaid in transparency are the SEVIRI droplet effective radius retrievals from SEVIRI
781 showing especially large droplets in the rift. Time series (7-10 August) of (b) CCN
782 concentrations at 0.12% and 0.4% supersaturation, and total aerosol concentration; (c) fraction of
783 time during each hour that clouds and drizzle are detected overhead; (d) liquid water path, error
784 bars indicating variability using standard deviation; (e) radar reflectivity (colors), cloud base
785 (filled black circles), inversion base (blue open circles) and inversion top (blue filled circles).

786 **Figure 12:** Time series of (a) CCN (red) and retrieved cloud droplet concentration N_d (blue); (b)
787 liquid water path (blue) and cloud base precipitation rate (red); (c) precipitation rate as a function
788 of height; also shown are radar-determined cloud top and ceilometer cloud bases; (d) radar
789 reflectivity; (e) lidar backscatter, for a case of low clouds observed on 7 November 2010.

790 **Figure 13**: Accumulated precipitation during the relatively dry month of Aug. 2009 and the
791 wetter month of Nov. 2009. Black shows rain gauge measurements at the Graciosa AMF site,
792 while the colors show model results interpolated to the site location from grid-cell means.

793 **Figure 14**: Time-height plots of daily-mean lower-tropospheric cloud fraction simulated by
794 models and AMF observed (based on the CloudNet cloud mask, Illingworth et al. 2007) for the
795 dry and the wet month.

796 **Figure 15**: Daily-mean CCN concentration at 0.1% supersaturation for the models and as
797 measured at the Graciosa site. The colored numbers for each month are temporal correlation
798 coefficients between log(CCN) for each model vs. the observations.

799
800
801
802
803

804

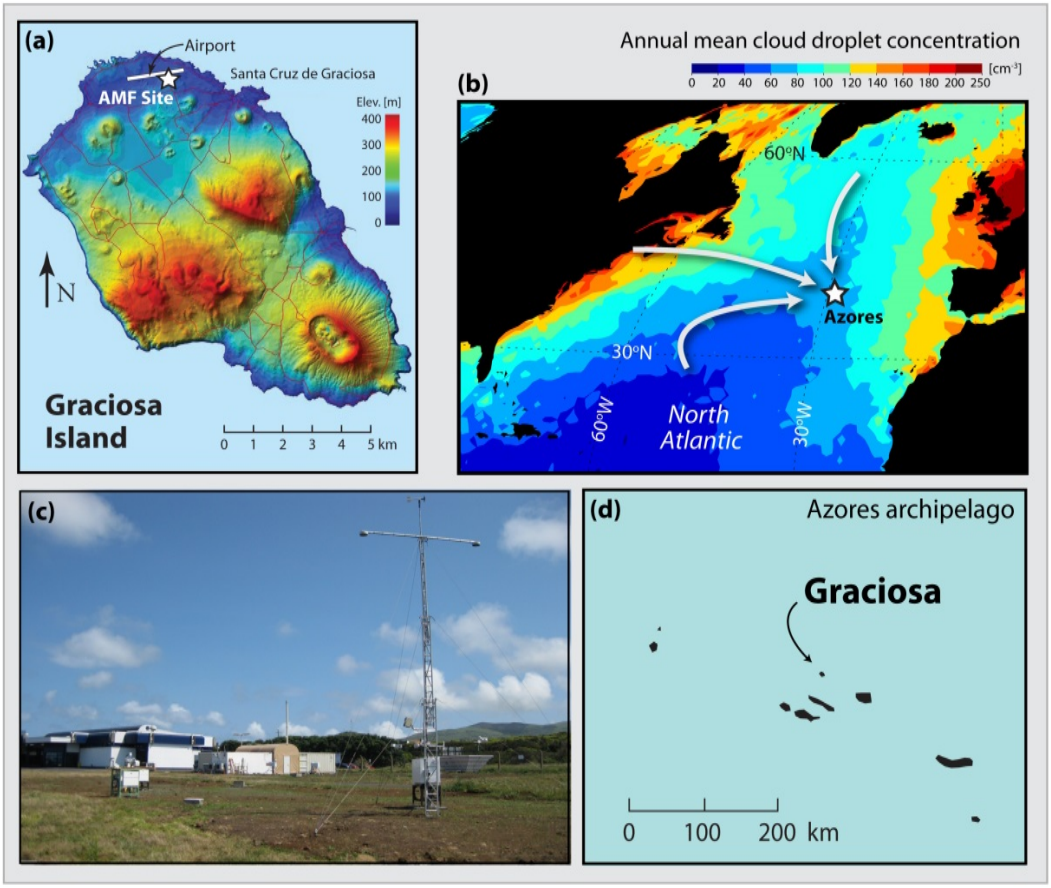

805

806 **Figure 1**: (a) Map of Graciosa Island showing terrain elevation, and the location of the AMF site
807 at the airport approximately 2 km west of the main town Santa Cruz de Graciosa. (b) Map
808 showing the location of the Azores in the North Atlantic. Colors show the annual mean cloud
809 droplet concentration for warm, overcast clouds as observed by the Moderate Resolution
810 Imaging Spectroradiometer (MODIS) on the NASA Terra satellite. The Azores receives a
811 diverse range of airmasses from North America, from the Arctic and from Northern Europe. (c)
812 Photograph of the AMF site looking to the SE; (d) Map of the location of Graciosa (and Pico) in
813 the Azores archipelago.
814

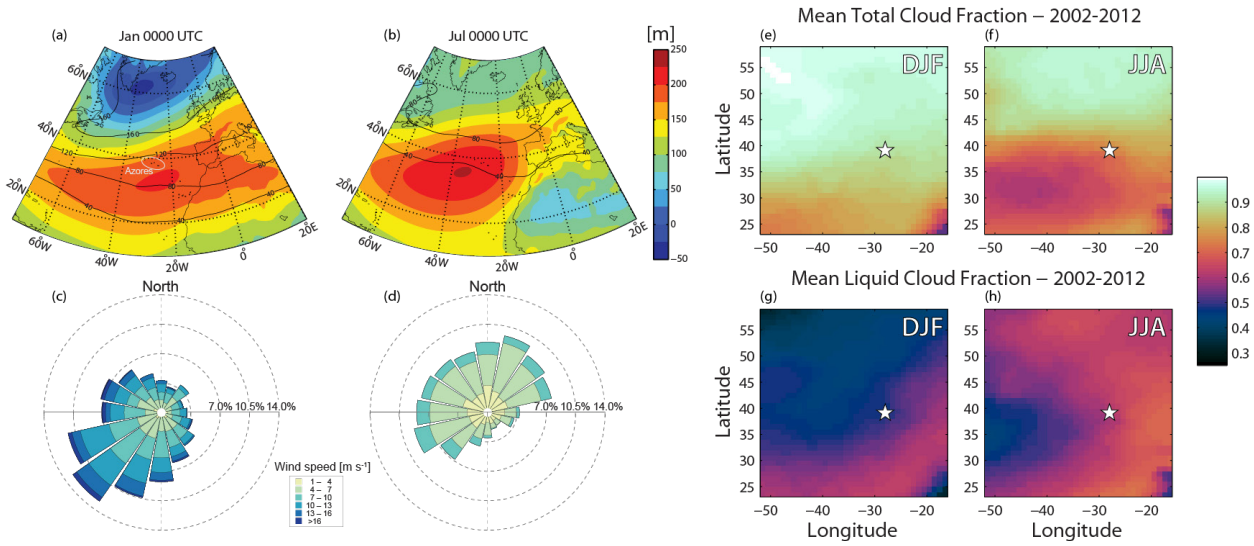

Figure 2: Mean 1000 hPa geopotential heights (color-filled contours) for (a) Jan. and (b) Jul. generated from the 0000 UTC ERA–Interim reanalysis fields (Dee et al. 2011). Contours of the standard deviation of the 500 hPa geopotential heights [in meters] are overlaid to indicate variability in the storm track. (c) and (d) represent surface wind roses for Jan. and July, respectively. (e)–(h) show maps of MODIS mean total and liquid phase cloud fraction for Dec., Jan., and Feb. (DJF) and Jun., Jul., and Aug (JJA) seasons. Cloud fraction is derived on 1°×1° areas averaged over each 3 month season for the years 2002-2012 using the Collection 51 Aqua MODIS Cloud Phase Infrared Day Histogram Counts product. Day and night observations are combined. The star in the cloud fraction panels denotes the location of Graciosa Island. A 3×3 pixel median smoothing filter was applied to the data to remove orbit swath edge sampling artifacts.

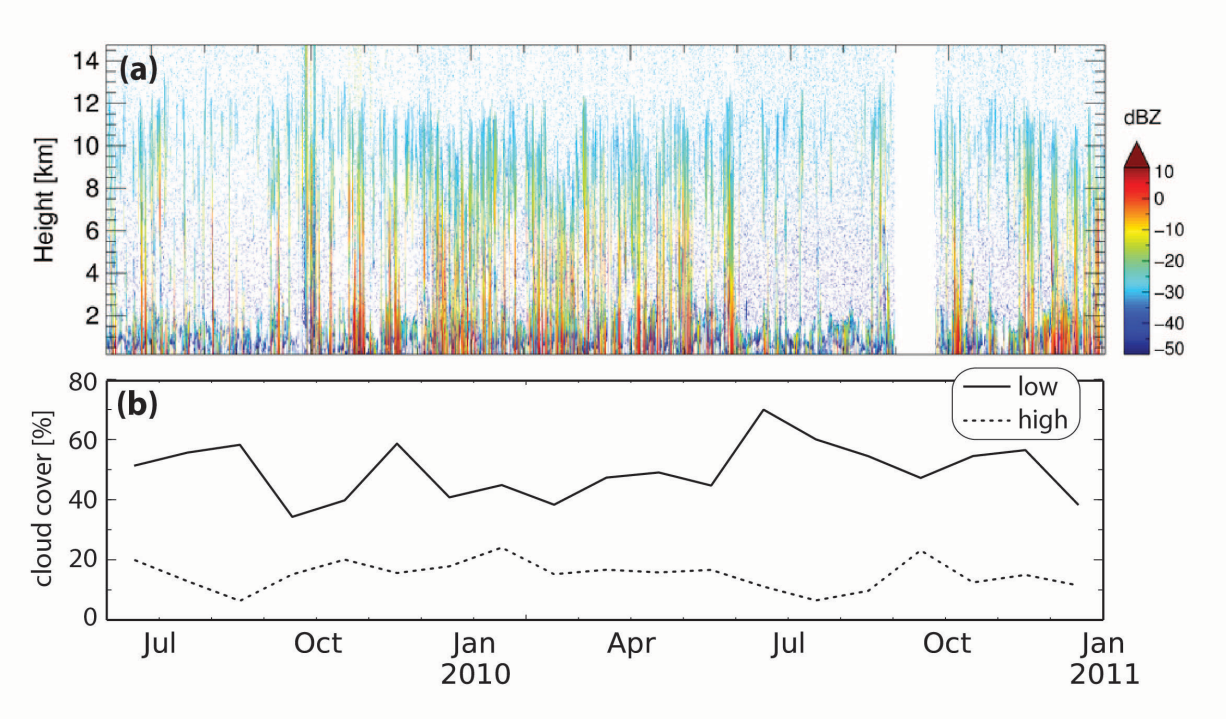

Figure 3: (a) height-time series of vertically-pointing W-band radar reflectivity for the entire deployment. Radar data for much of September 2010 are missing; (b) monthly low and high cloud cover determined using the WACR and ceilometer dataset as described in Rémillard et al. (2012).

844

845

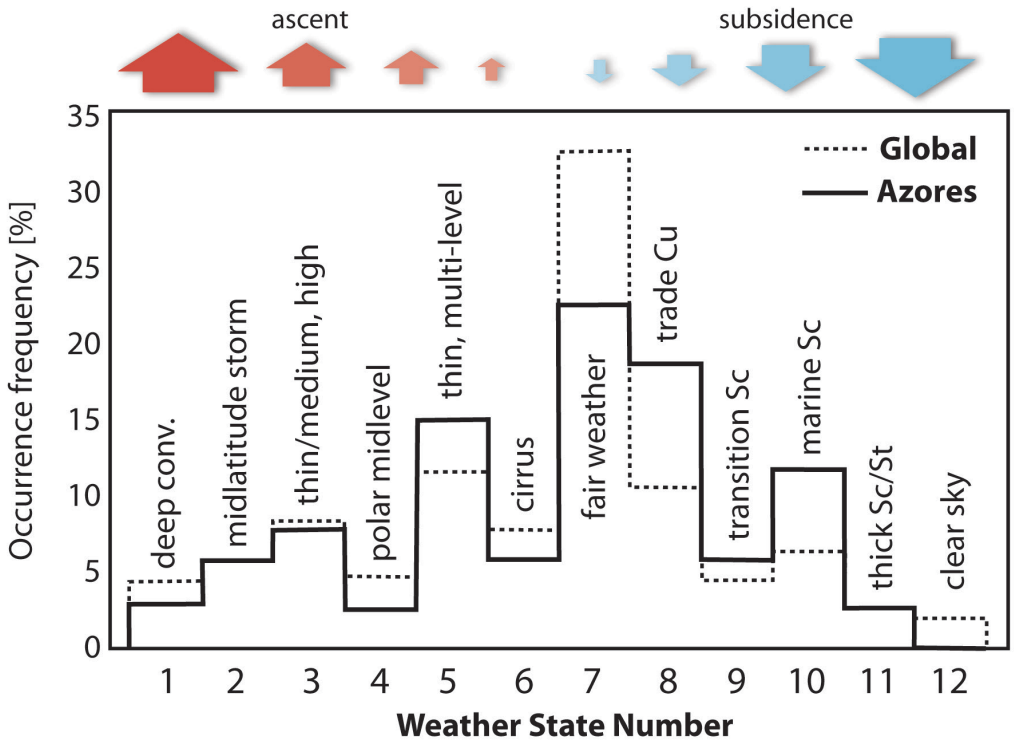

846

847 **Figure 4**: Frequency of occurrence of different weather states determined using passive and
848 active cloud sensors at the Azores (solid) and for the globe as a whole (dotted). From Tselioudis
849 et al. (2013).

850

851

852

853

854

855

856

857

858

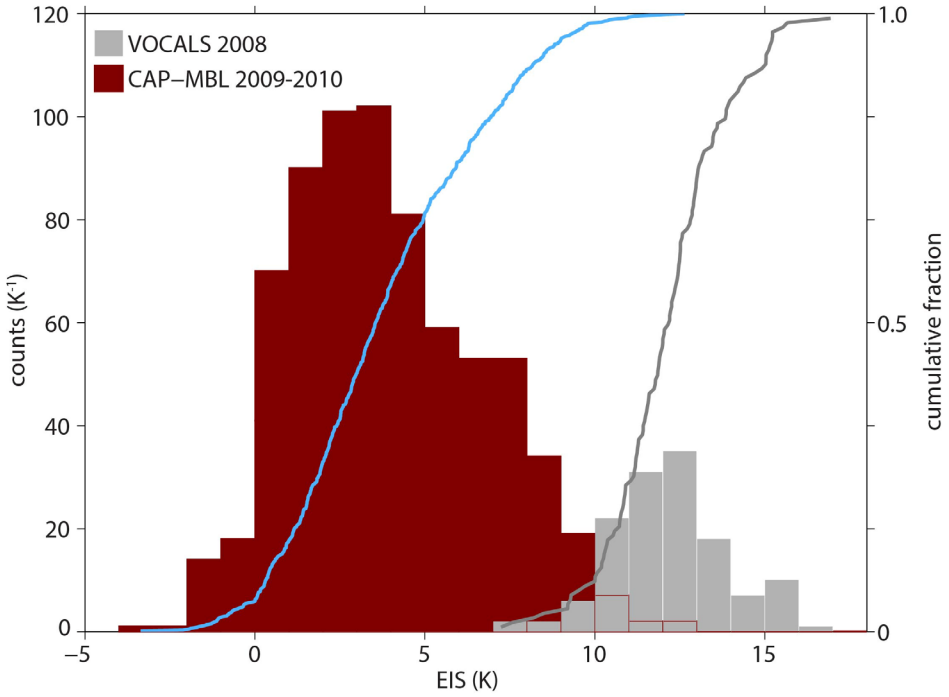

859

860 **Figure 5**: Histogram counts of estimated inversion strength (EIS, Wood and Bretherton 2006) in
861 1 K bins from summertime (June-August) CAP-MBL 2009 and 2010 soundings (red bars) and
862 VOCALS 2008 (October-November, gray bars). Right axis shows cumulative distributions of
863 EIS for all of CAP-MBL (blue line) and VOCALS (gray line).

864

865

866

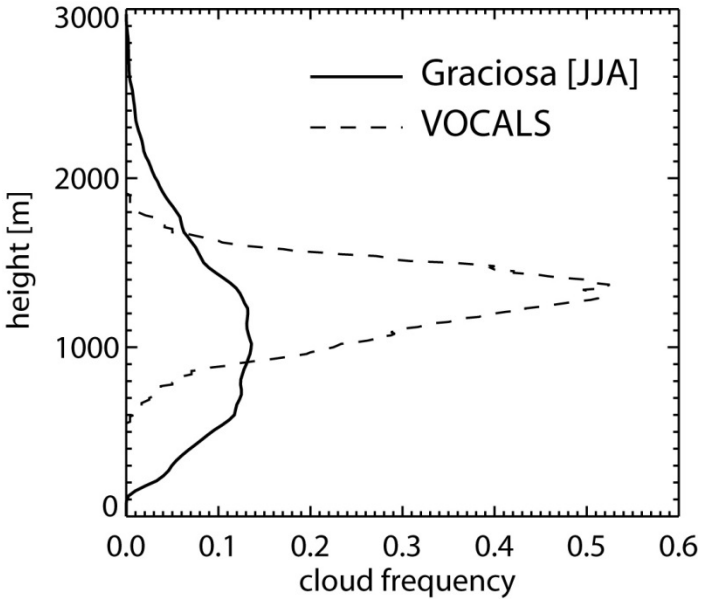

867

868 **Figure 6**: Cloud occurrence frequency as a function of height for Graciosa during JJA (solid)
869 and from the southeastern Pacific during the VOCALS field campaign (Burleyson et al. 2013).

870

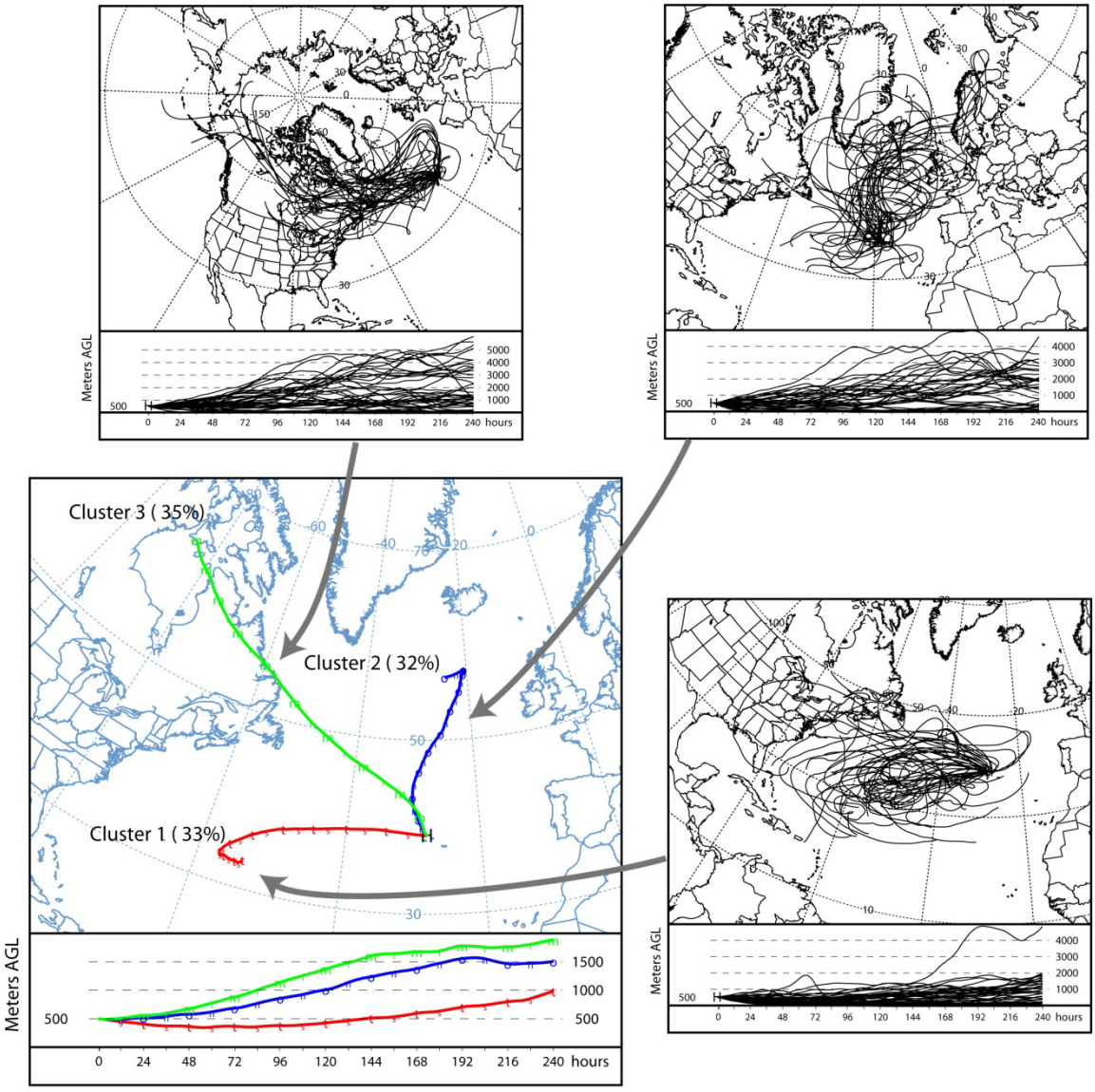

Figure 7: Clusters of trajectories arriving at Graciosa during the summer period (May-August 2009) showing the three primary clusters representing North American, Arctic/Northern European, and recirculating Azores high flow. The Hysplit IV model (Draxler and Rolph, 2003) was employed and 10 day back trajectories ending at Graciosa 500 m above sea level were run every day for April-September 2009. NCEP GDAS meteorological data including model vertical velocity is used to determine the trajectory motion. A cluster analysis was then performed on the resulting back trajectory set (e.g., Toledano et al., 2009) and a three cluster solution was found to capture most of the variance.

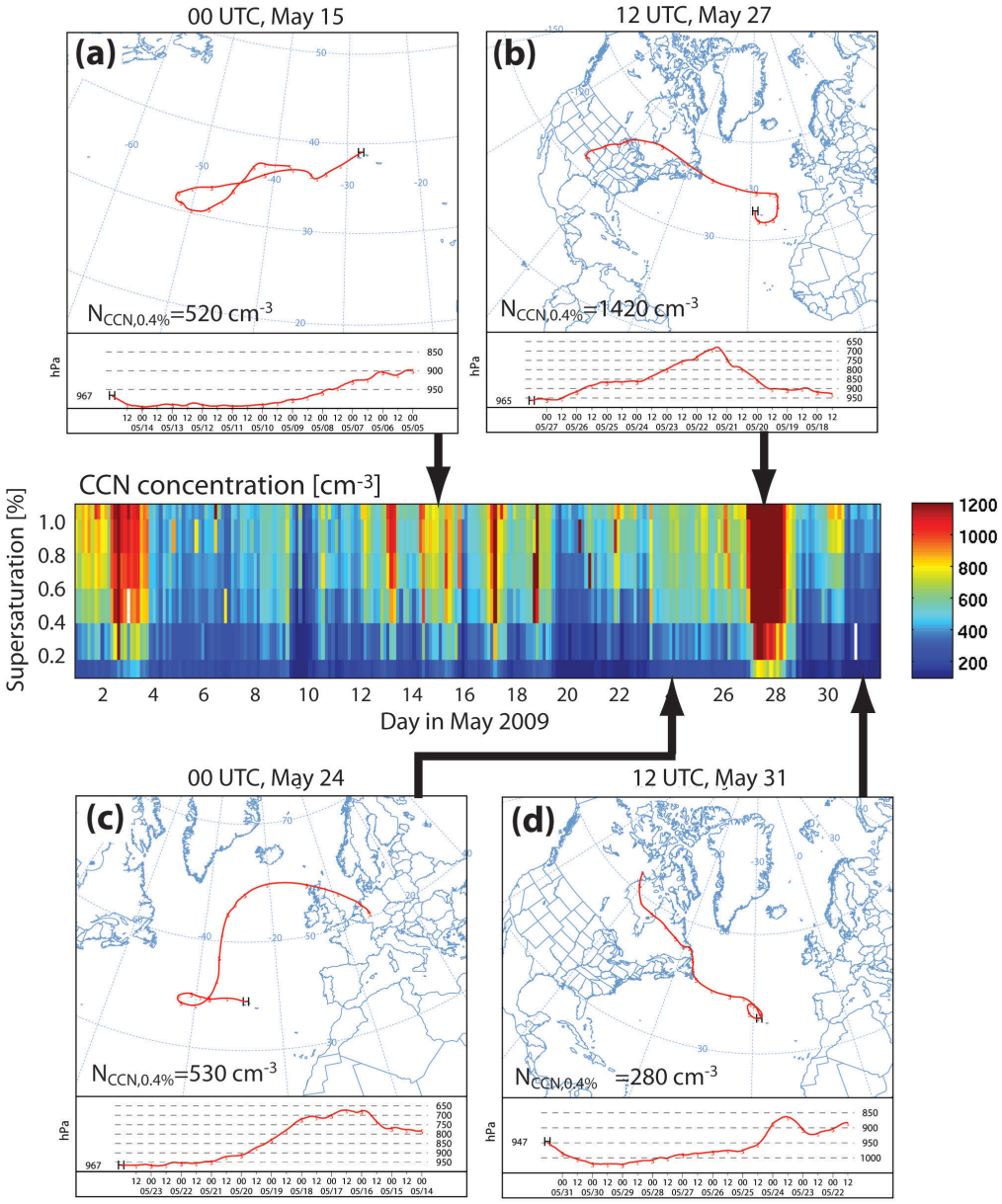

882

883

884 **Figure 8**: (a)-(d) Four examples of 10 day airmass back trajectories (see Fig. 7 caption for
885 details) arriving at Graciosa during May 2009, reflecting characteristic airmasses. Each of the
886 four panels show the trajectory map (top) and height (below) with ticks every 12 hours. Central
887 panel shows CCN supersaturation spectra time series measured at Graciosa during the same
888 month.

889

890

891

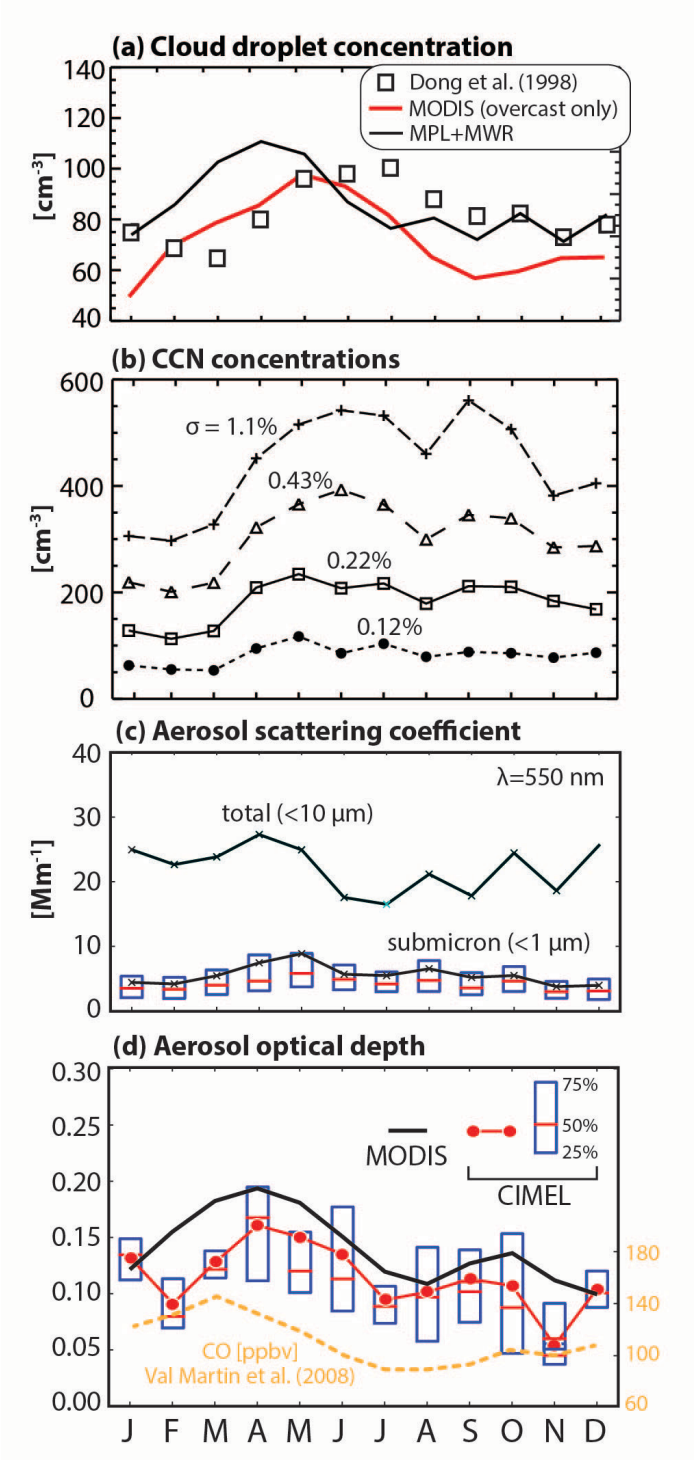

Figure 9: Composite seasonal cycles (using all available data) of (a) cloud droplet concentration retrieved using the transmitted solar irradiance and microwave radiometer (MWR) LWP (squares, Dong et al. 1998), from the MPL solar background light (Chiu et al. 2007) and MWR (black line), and from MODIS (red line, 1x1° box encompassing Graciosa, all years 2001-2010, Platnick et al. 2003); (b) Surface CCN concentrations at four supersaturations; (c) Aerosol total and submicron dry extinction. Boxes span the 25th and 75th percentiles of the data with red bars indicating medians and the crosses indicating means; (d) Monthly mean aerosol optical depth and 25/50/75th percentile values from the sunphotometer (CIMEL, red) and mean values from MODIS (black). The composite seasonal cycle of carbon monoxide (CO) measured at the Pico mountain station from 2002 to 2005 is also shown (see Val Martin et al. 2008).

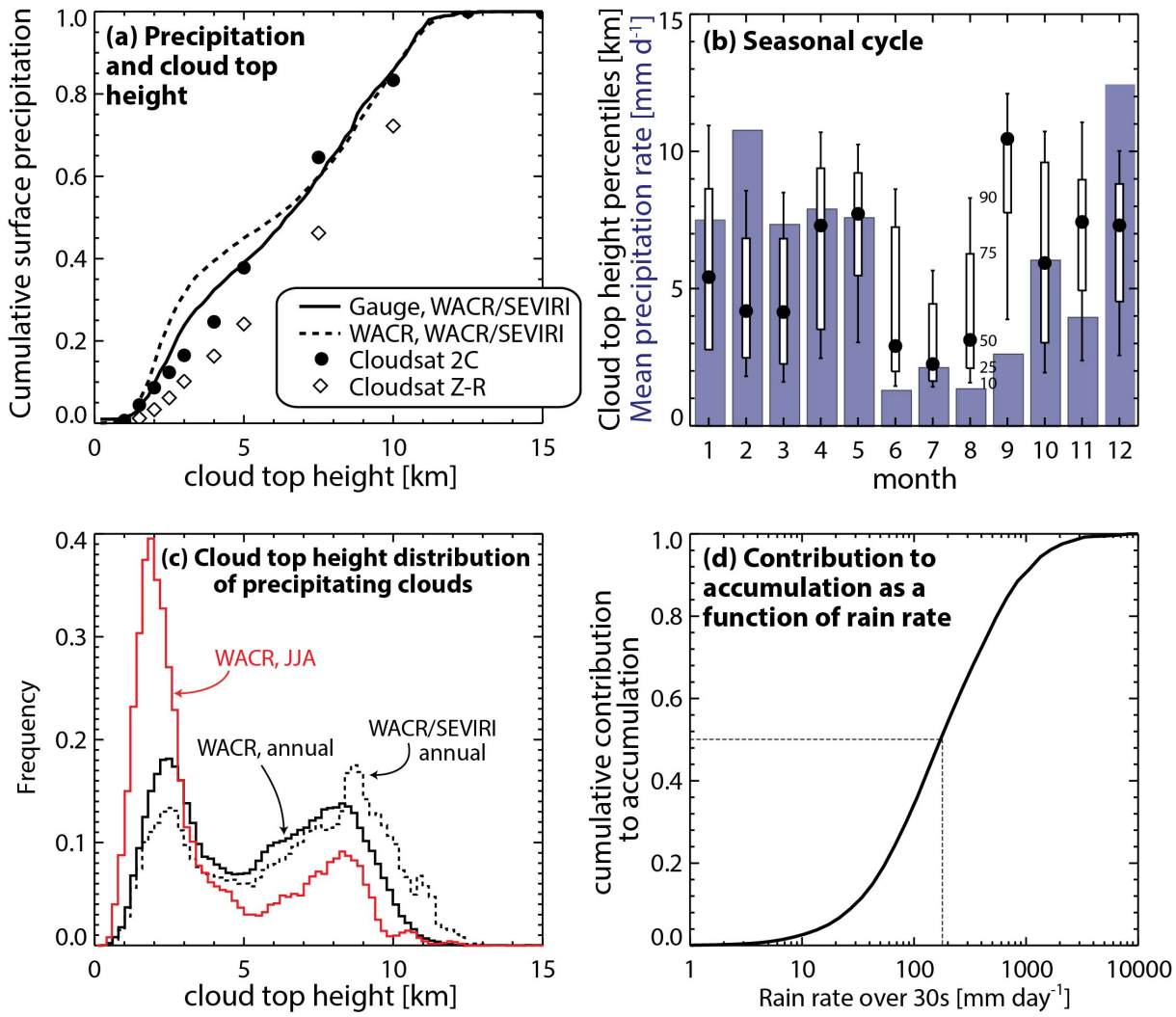

Figure 10: Characteristics of precipitation reaching the surface at Graciosa. (a) Cumulative contribution to surface precipitation accumulation from clouds with tops exceeding the value shown on the abscissa, using different approaches. The solid line shows precipitation determined by the raingauge and cloud top height estimated with WACR for columns that are not completely attenuated and satellite-determined IR cloud top height from SEVIRI for attenuated columns. Filled circles are from CloudSat. (b) composite seasonal cycle of precipitation from 21 months of the deployment (blue bars), and the cloud top height corresponding to percentiles of total precipitation accumulation. For example, the filled circles indicate the cloud top height for which 50% of the total precipitation is associated with shallower clouds. (c) Cloud top height distributions corresponding to 30 s periods where the surface precipitation exceeds 10 mm d^{-1}. Black solid line shows cloud tops from the WACR only and the dotted line shows those from WACR/SEVIRI merge, both for annual data. The red curve shows corresponding plot for JJA. (d) Contribution to surface accumulation from precipitation rates exceeding the abscissal value.

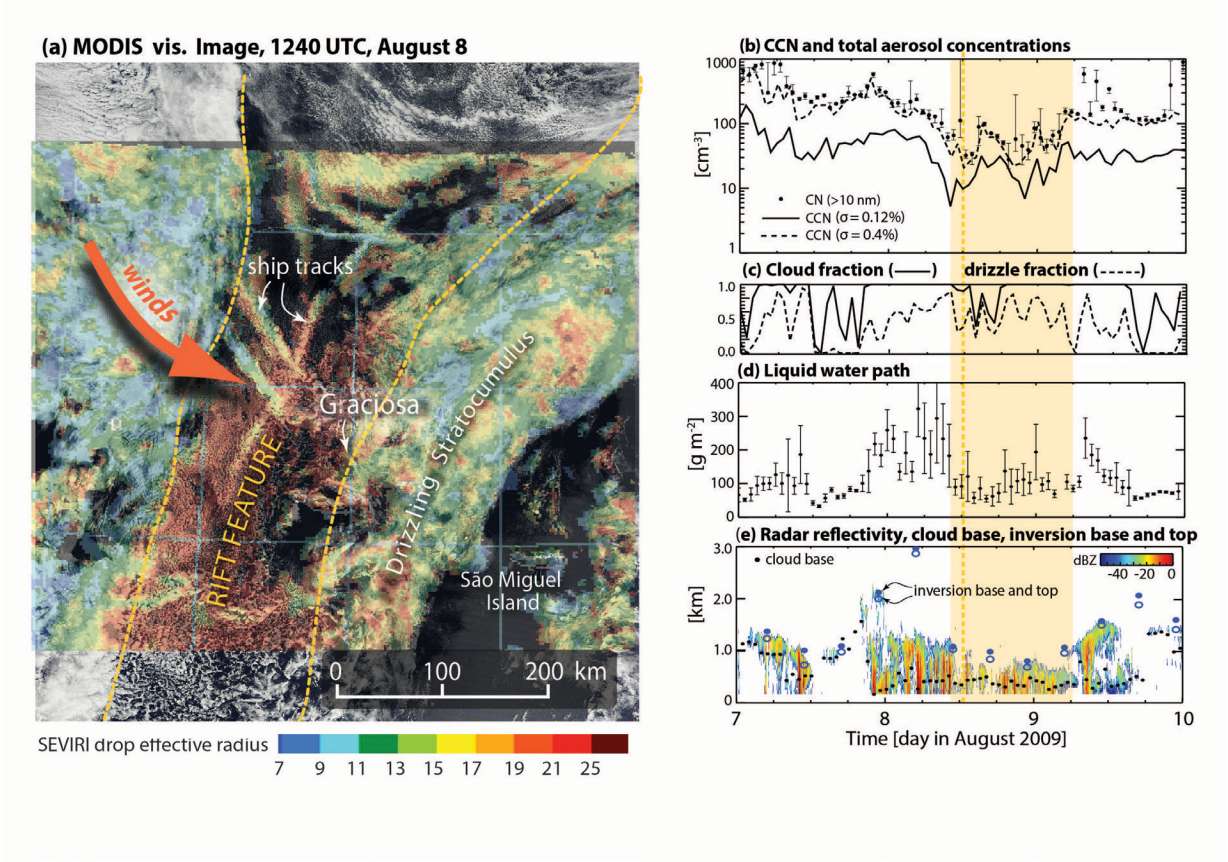

957

958 **Figure 11**: (a) MODIS visible image on 8 August 2009 (12:40 UTC) showing rift feature
959 containing small open cells and shiptracks in a shallow boundary layer about to cross Graciosa.
960 Overlaid in transparency are the droplet effective radius retrievals from SEVIRI showing
961 especially large droplets in the rift. Time series (7-10 August) of (b) CCN concentrations at
962 0.12% and 0.4% supersaturation, and total aerosol concentration; (c) fraction of time during each
963 hour that clouds and drizzle are detected overhead; (d) liquid water path, error bars indicating
964 variability using standard deviation; (e) radar reflectivity (colors), cloud base (filled black
965 circles), inversion base (blue open circles) and inversion top (blue filled circles).
966
967
968
969
970
971
972
973

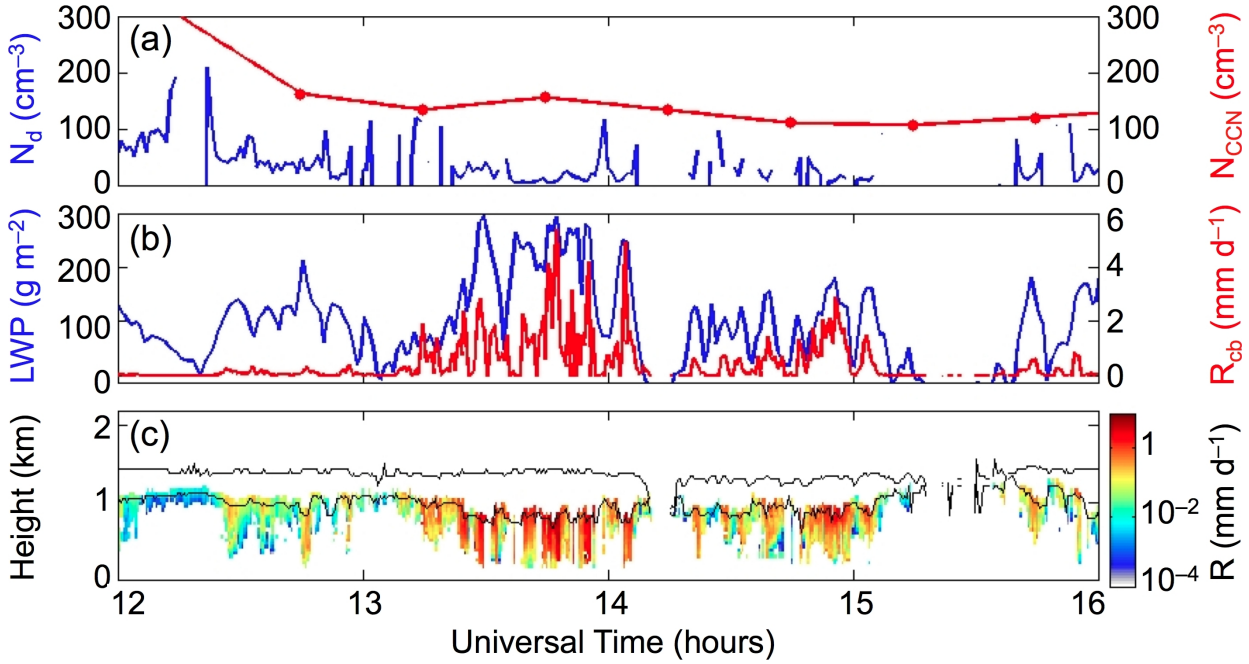

Figure 12: Time series of (a) CCN (red) and retrieved cloud droplet concentration N_d (blue); (b) liquid water path (blue) and cloud base precipitation rate (red); (c) precipitation rate as a function of height; also shown are radar-determined cloud top and ceilometer cloud bases, for a case of low clouds observed on 7 November 2010.

981

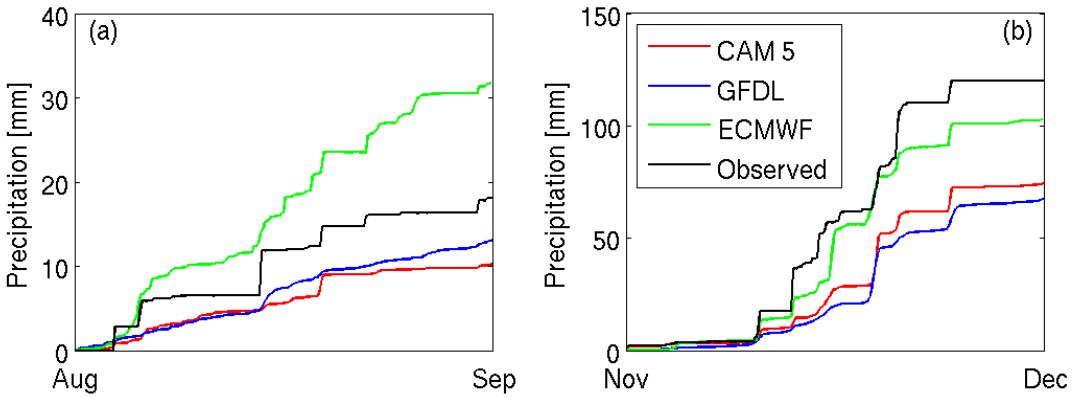

982

983 **Figure 13**: Accumulated precipitation during the relatively dry month of Aug. 2009 and the
984 wetter month of Nov. 2009. Black shows rain gauge measurements at the Graciosa AMF site,
985 while the colors show model results interpolated to the site location from grid-cell means.

986

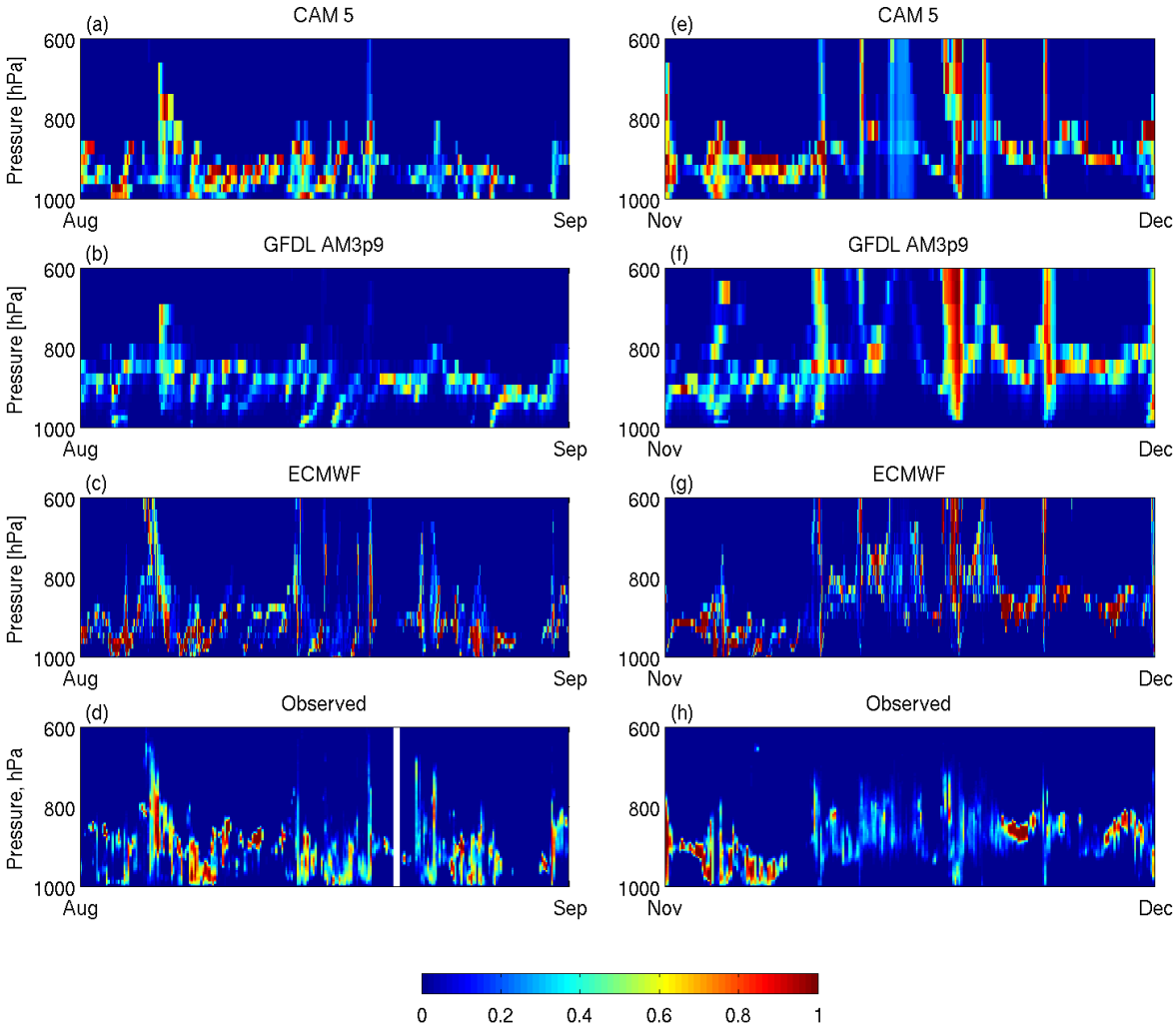

Figure 14: Time-height plots of daily-mean lower-tropospheric cloud fraction simulated by models and AMF observed (based on the CloudNet cloud mask, Illingworth et al. 2007) for the dry and the wet month.

993

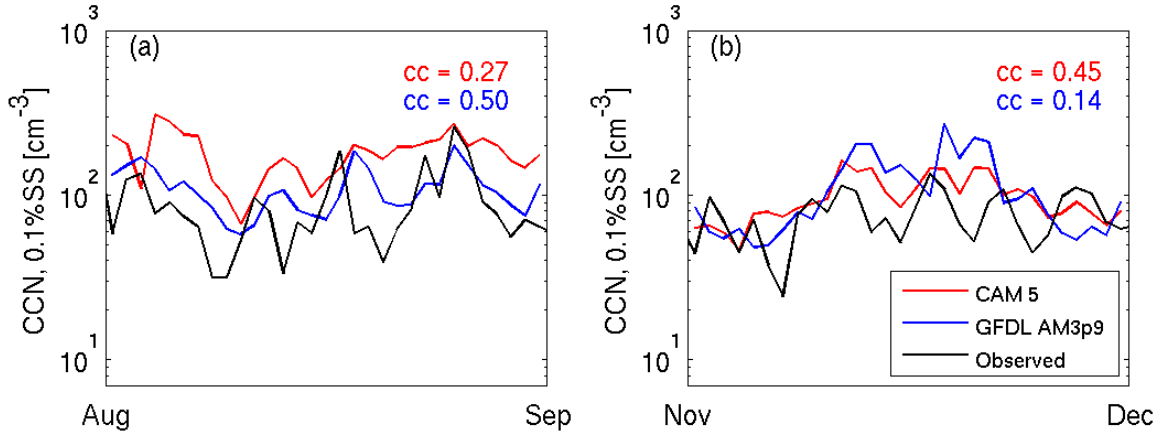

994

995 **Figure 15**: Daily-mean CCN concentration at 0.1% supersaturation for the models and as
996 measured at the Graciosa site. The colored numbers for each month are temporal correlation
997 coefficients between log(CCN) for each model vs. the observations.

998

999